Correlating the Arperos Basin from Guanajuato, central Mexico, to Santo Tomás, southern Mexico: Implications for the paleogeography and origin of the Guerrero terrane

Michelangelo Martini[1,*], Luigi Solari[2], and Margarita López-Martínez[3]
[1]*Instituto de Geología, Universidad Nacional Autónoma de México, 04510, México D.F., México*
[2]*Centro de Geociencias, Universidad Nacional Autónoma de México, Campus Juriquilla, 76230, Querétaro, México*
[3]*Laboratorio de Geocronología, División de Ciencias de la Tierra, CICESE, 22860, Ensenada, Baja California, México*

ABSTRACT

The Guerrero terrane has been interpreted either as a Mesozoic Pacific multi-arc system accreted to North America, or as a detached slice of the North American continental margin, which was rifted during backarc spreading and subsequently accreted back to the continental mainland. In order to test these two scenarios, we present here a petrologic study of metasandstones from the Santo Tomás area, southern Mexico. Our data document that the Guerrero terrane suture belt contains the remnants of the Tithonian–Cenomanian Arperos Basin. This basin displays a marked provenance asymmetry. Its eastern margin is composed of metasedimentary rocks derived from sources in the North American continental mainland, whereas its western margin consists of a metasedimentary succession derived from volcanic sources of the Guerrero terrane. Sedimentation in the Arperos Basin was coeval with the emplacement of Tithonian–Barremian felsic dikes and lava flows with volcanogenic massive sulfide deposits and Aptian–Cenomanian intraplate-like and mid-ocean ridge basalts. This suggests that the Arperos Basin evolved progressively from continentally to oceanic floored during the Early Cretaceous and that a mature oceanic crust was generated only ca. 15 Ma before the accretion of the Guerrero terrane, which took place in the late Cenomanian. On the basis of this evidence, we favor a North American origin for the Guerrero terrane, which is then considered to represent a west-facing North American arc that was rifted from the continental mainland during backarc spreading and subsequently accreted back to nuclear Mexico.

INTRODUCTION

The Guerrero terrane extends for ~1500 km along the Pacific margin of Mexico (Fig. 1), and it represents the second largest terrane of the North American Cordillera (Campa and Coney, 1983; Coney et al., 1980). This terrane is composed of an Upper Triassic metamorphic basement named the Arteaga Complex, which is unconformably overlain by Bajocian–Cenomanian submarine arc assemblages accreted to the North American continental mainland between the Albian and Cenomanian (Centeno-García et al., 2003; Talavera-Mendoza et al., 2007; Centeno-García et al., 2008; Martini et al., 2011). Scattered outcrops of highly sheared and folded metaturbidites interbedded with intraplate-like and mid-ocean ridge (MOR) basalts are exposed along the eastern boundary of the Guerrero terrane at Zacatecas, Guanajuato, Santo Tomás, and Arcelia (Tardy et al., 1994; Freydier et al., 1996; Mendoza and Suástegui, 2000; Martini et al., 2011) (Fig. 1). These rocks have been interpreted as the vestiges of an inverted

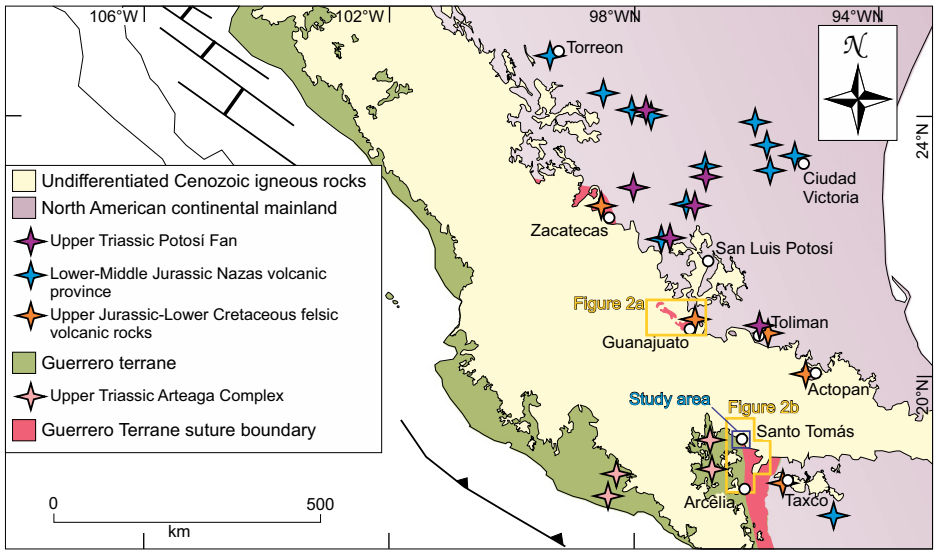

Figure 1. Schematic map of Mexico showing the location and extension of the North American continental mainland and the Guerrero terrane. Distribution of the Upper Triassic Potosí Fan and Arteaga Complex is depicted in the figure, as well as exposures of Lower Jurassic–Lower Cretaceous volcanic rocks of the continental mainland.

*mmartini@geologia.unam.mx

Geosphere; December 2014; v. 10; no. 6; p. 1385–1401; doi:10.1130/GES01055.1; 13 figures; 3 tables; 1 supplemental file.
Received 22 March 2014 ♦ Revision received 19 July 2014 ♦ Accepted 10 August 2014 ♦ Published online 7 October 2014

oceanic basin named Arperos Basin, which was originally interposed between the Guerrero terrane and the North American mainland margin (Tardy et al., 1994). Different paleogeographic and geodynamic scenarios have been proposed for the Arperos Basin and the Guerrero terrane and can be summarized in two different groups. Group 1 comprises the models that considered the Arperos Basin a part of the paleo-Pacific plate (Tardy et al., 1994; Dickinson and Lawton, 2001; Talavera-Mendoza et al., 2007). According to these scenarios, the Guerrero terrane is interpreted as an exotic Pacific arc (Tardy et al., 1994; Dickinson and Lawton, 2001) (Fig. 2A) or a North America–fringing multi-arc system developed on a paleo-Pacific oceanic substrate that received sediments from the continental margin (Talavera-Mendoza et al., 2007) (Fig. 2B). Alternatively, scenarios of group 2 consider the Arperos Basin an oceanic backarc basin developed along the continental margin of North America (Cabral-Cano et al., 2000; Elías-Herrera et al., 2000; Centeno-García et al., 2008; Martini et al., 2011) (Fig. 2C). According to group 2 scenarios, the Guerrero terrane was developed on Upper Triassic metamorphic rocks of the North American continental margin and was rifted in the Early Cretaceous during backarc extension.

Resolving the controversy on the origin of the Guerrero terrane and Arperos Basin is fundamental in reconstructing the paleogeography of southwestern North America and contributes to an understanding of the tectonic processes that shaped the margins of the continental masses. In order to test the North American and Pacific paleogeographic scenarios proposed for the Arperos Basin, we present in this paper a combined study that includes detailed mapping, sandstone provenance analysis, U-Pb, and $^{40}Ar/^{39}Ar$ geochronology of an exposure of the Guerrero suture belt in the Santo Tomás area, southern Mexico (Fig. 1).

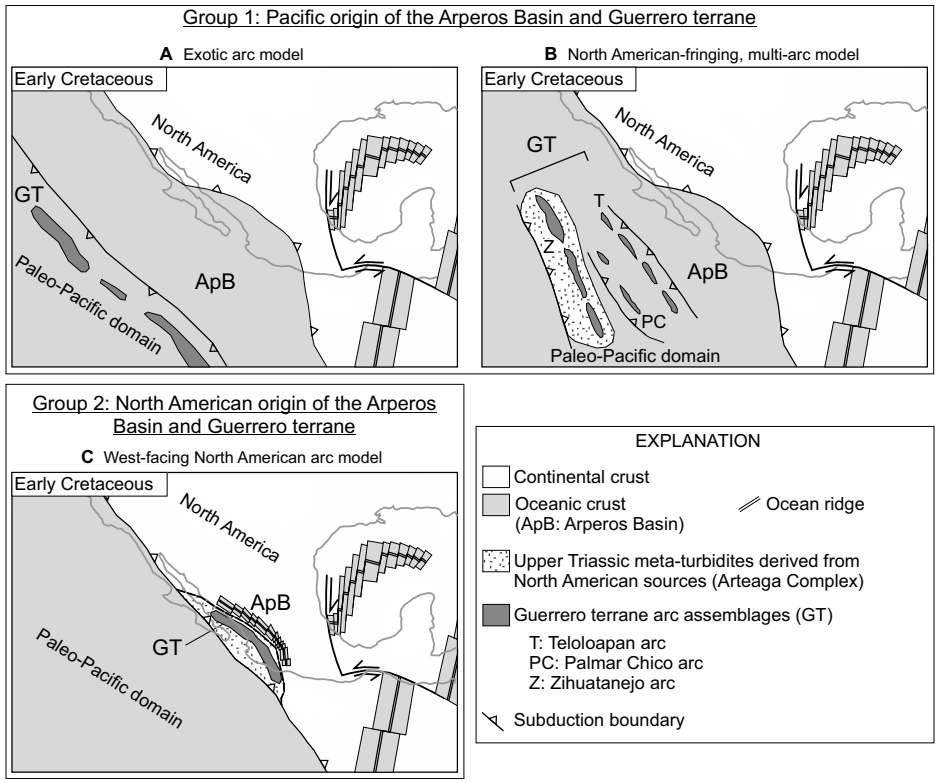

Figure 2. Paleogeographic reconstructions proposed by previous authors for the Arperos Basin and Guerrero terrane. Group 1 scenarios (A and B) consider the Arperos Basin part of the paleo-Pacific oceanic plate. Consequently, the Guerrero terrane is interpreted as (A) a Pacific exotic arc (Tardy et al., 1994; Dickinson and Lawton, 2001) or as (B) a North American–fringing multi-arc system, which was developed on a paleo-Pacific oceanic substrate that received sediments from the continental margin (Talavera-Mendoza et al., 2007). Alternatively, scenarios of group 2 (C) consider the Arperos Basin as an oceanic backarc basin developed along the North American continental margin. According to these scenarios, the Guerrero terrane was developed on Upper Triassic metamorphic rocks of the North American continental margin and was rifted in the Early Cretaceous during backarc extension (Cabral-Cano et al., 2000; Elías-Herrera et al., 2000; Centeno-García et al., 2008; Martini et al., 2011).

GEOLOGICAL OVERVIEW OF THE ARPEROS BASIN

Central Mexico

In central Mexico, the Arperos Basin is exposed at Guanajuato (Figs. 1 and 3A) and is presently arranged in a complex fold-thrust belt representing the suture between the North American continental mainland and the Guerrero terrane (Tardy et al., 1994; Martini et al., 2013). At Guanajuato, the Arperos Basin displays a marked provenance asymmetry. The eastern margin of this basin is composed of Tithonian–Aptian quartz-rich and calcareous metaturbidites of the Esperanza assemblage, which were derived from sources in the North American continental mainland (Martini et al., 2012; Palacios-García and Martini, 2014). Such a provenance is highlighted by the presence of ca. 210–300, ca. 450–700, and ca. 900–1650 Ma detrital zircon derived from Upper Triassic, quartz-rich metaturbidites of the Potosí Fan (Fig. 1), ca. 200–164 Ma zircon grains sourced from the Early-Middle Jurassic Nazas volcanic province (Fig. 1), and a ca. 150–130 Ma zircon population derived from Upper Jurassic–Lower Cretaceous rhyodacitic volcanic rocks localized at Guanajuato and Toliman (Martini et al., 2012; Palacios-García and Martini, 2014) (Fig. 1). On its western margin, the Arperos Basin is made up of Aptian volcaniclastic metaturbidites of the Arperos assemblage that were derived from sources within the Guerrero terrane (Martini et al., 2012) (Fig. 3A). Metaturbidites of the western Arperos assemblage contain ca. 160–118 Ma detrital zircons derived from the Guerrero terrane arc assemblages and subordinate Middle Triassic to Mesoproterozoic grains sourced from Upper Triassic metaturbidites of the Arteaga Complex (Martini et al., 2012).

U-Pb geochronologic and geochemical analyses indicate that the sedimentation in the Arperos Basin was coeval with the emplacement of Tithonian rhyodacitic dikes and lava flows hosting volcanogenic massive sulfide (VMS) deposits and Lower Cretaceous intraplate-like and MOR metabasalts (Ortíz-Hernández et al., 1992; Freydier et al., 1996; Mortensen et al., 2008; Martini et al., 2011).

According to paleontologic and U-Pb geochronologic data, the Arperos Basin in the Guanajuato area was closed during the late Aptian, and it was finally overthrust by the El

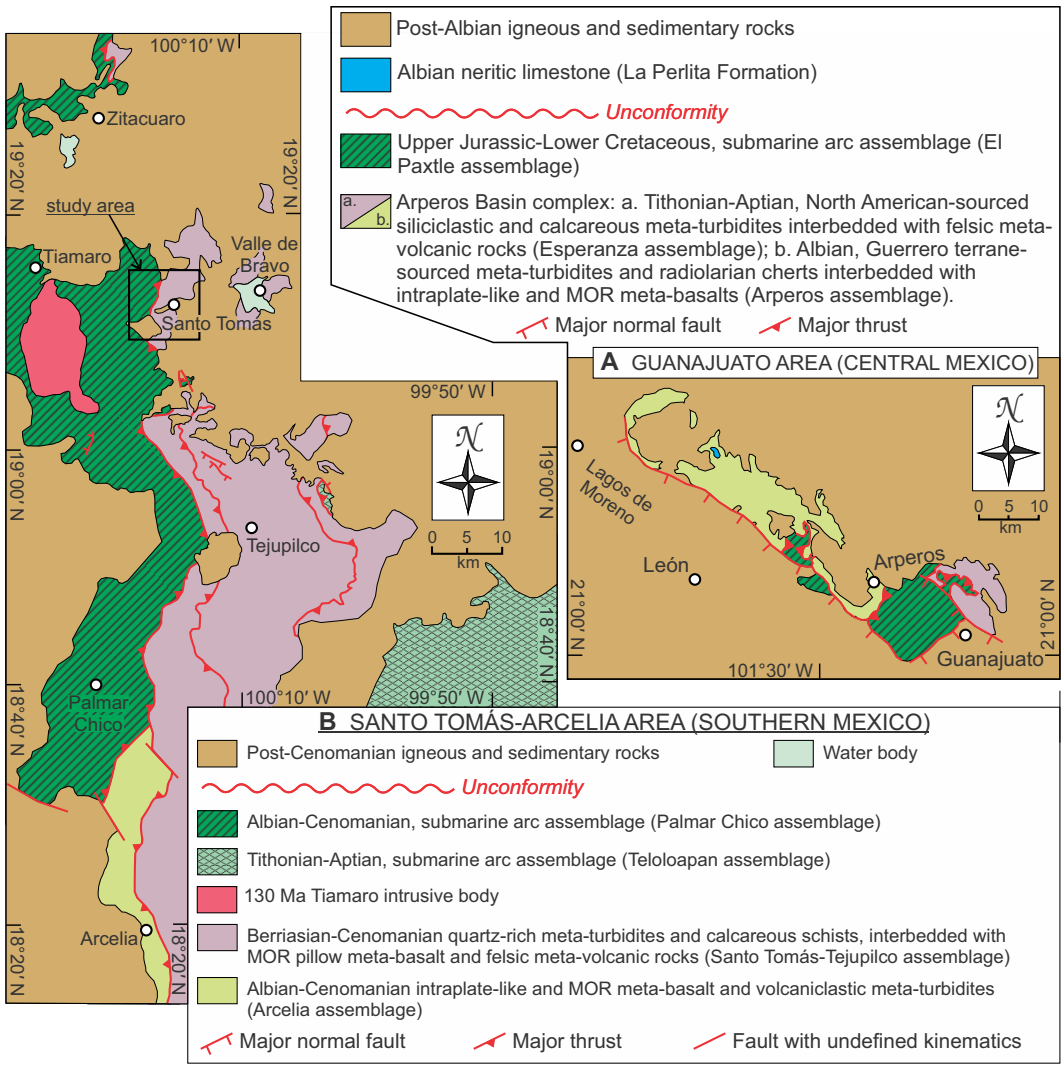

Figure 3. Schematic geologic maps of the Guanajuato (A) and Santo Tomás–Arcelia (B) areas, showing the distribution and contact relationships of the different tectono-stratigraphic assemblages exposed across the boundary of the Guerrero terrane in central and southern Mexico. Map of the Guanajuato area is modified by Martínez-Reyes (1992) and Martini et al. (2012). Map of the Santo Tomás–Arcelia area is recompiled based on Freydier et al. (1996), Elías-Herrera et al. (2000), Mendoza and Suástegui (2000), Fitz-Díaz et al. (2008), and available maps published by the Mexican Geological Survey. MOR—mid-ocean ridge.

Paxtle submarine arc assemblage of the Guerrero terrane with a top-to-the-NE main direction of tectonic transport (Chiodi et al., 1988; Lapierre et al., 1992; Ortíz-Hernández et al., 1992; Tardy et al., 1994; Martini et al., 2011) (Fig. 3A).

Southern Mexico

In southern Mexico, the architecture, depositional evolution, and sedimentary provenance of the Arperos Basin have not been previously assessed. Possible exposures of the Arperos Basin were tentatively proposed by Freydier et al. (1996) based on the reconnaissance of Lower Cretaceous calcareous metaturbidites interbedded with MOR metabasalts in the Santo Tomás area (Figs. 1 and 3B). The succession described by Freydier et al. (1996) was successively analyzed in detail in the Tejupilco area (Fig. 3B) and was described as a metavolcano-sedimentary assemblage of the Guerrero terrane, composed of quartz-rich metaturbidites and calcareous schists, interbedded with MOR pillow metabasalts and metarhyolites with VMS deposits (Elías-Herrera et al., 2000; Mortensen et al., 2008; Elías-Herrera et al., 2009). Available paleontologic and geochronologic data constrain the age of the Santo Tomás–Tejupilco assemblage in the Berriasian–Cenomanian (Cantú-Chapa, 1968; Israde-Alcantara and Martínez-Alvarado, 1986; Elías-Herrera et al., 2000; Elías-Herrera et al., 2009).

Another metavolcano-sedimentary assemblage containing intraplate-like and MOR metabasalts has been described in the surroundings of Arcelia, 60 km south of Tejupilco (Mendoza and Suástegui, 2000) (Fig. 3B). However, its possible correlation with the successions of the Arperos Basin was not explored. The Arcelia assemblage is composed of pillow and massive metabasalt, basaltic breccia, and hyaloclastite overlain by volcaniclastic metaturbidites and radiolarian cherts. These rocks are tectonically emplaced on the metavolcano-sedimentary assemblage of Santo Tomás–Tejupilco with a top-to-the-NE main direction of tectonic transport (Mendoza and Suástegui, 2000; Salinas-Prieto et al., 2000). The age of the Arcelia assemblage is constrained in the Albian–Cenomanian by a radiolarian fauna (Dávila-Alcocer and Guerrero-Suástegui, 1990).

The Santo Tomás–Tejupilco and Arcelia assemblages are tectonically overlain to the west and east by submarine volcanic arc assemblages that were emplaced with a top-to-the- NE main direction of tectonic transport (Mendoza and Suástegui, 2000; Elías-Herrera, 2004; Fitz-Díaz et al., 2008). The arc assemblage exposed east of Tejupilco was referred to as the Teloloapan arc assemblage, and it is composed of Tithonian–Aptian, calc-alkaline pillow and massive metabasalts, basaltic breccia, and radiolarian chert (Mendoza and Suástegui, 2000), which

are locally interlayered with ca. 150–139 Ma rhyolitic lava flows hosting VMS deposits (Mortensen et al., 2008). The arc assemblage to the west of Tejupilco was named the Palmar Chico assemblage and is composed of a succession lithologically and geochemically comparable to the one described for the Teloloapan assemblage (Mendoza and Suástegui, 2000). However, available $^{40}Ar/^{39}Ar$ ages from mafic metavolcanic rocks of the Palmar Chico assemblage vary from 114 to 93 Ma (Delgado-Argote et al., 1992; Elías-Herrera et al., 2000), hindering any possible stratigraphic correlation with the Tithonian–Aptian Teloloapan assemblage. A granitic to gabbroic intrusive body exposed near Tiamaro, in the northern part of the Palmar Chico assemblage (Fig. 3B), yielded U-Pb ages of ca. 130 Ma (Garza-González, 2007; Martini et al., 2009). However, these ages have not been considered in previous tectono-stratigraphic reconstructions and paleogeographic models. Therefore, based on the Albian–Cenomanian age assumed for the Palmar Chico assemblage, Talavera-Mendoza et al. (2007) developed the idea that the Santo Tomás–Tejupilco and Arcelia assemblages were deposited in a relatively narrow intraoceanic basin limited by two distinct arc massifs of the Guerrero terrane and exclude a correlation with the paleogeographic scenario defined for the Arperos Basin in central Mexico.

TECTONO-STRATIGRAPHIC FRAMEWORK OF THE SANTO TOMÁS AREA

The Santo Tomás area is located in southern Mexico, ~40 km north of Tejupilco (Fig. 3B). This area is of particular interest because it contains a volcano-sedimentary assemblage that was tentatively correlated to the succession of the Arperos Basin at Guanajuato (Freydier et al., 1996). Therefore, the Santo Tomás area is important in the search for a possible paleogeographic connection between central and southern Mexico, and may contribute to understand the origin and evolution of the Arperos Basin and the Guerrero terrane.

Three different tectono-stratigraphic assemblages are exposed in the Santo Tomás area and are arranged in a complex fold-thrust belt. These tectono-stratigraphic assemblages are: the Santo Tomás–Tejupilco, the Palmar Chico, and the Ojo de Agua assemblage (Figs. 4 and 5). The Santo Tomás–Tejupilco assemblage occupies the lowermost exposed structural levels (Figs. 4 and 5), and it is composed of low-grade, greenschist-facies calcareous schist and phyllite, alternating with scarce siliciclastic metasandstone and pillow metabasalt (Fig. 5). Relics of primary structures are very scarce in metasedimentary rocks. Locally, ripple lamination was observed in calcareous schists, indicating that these strata were deposited by submarine traction currents.

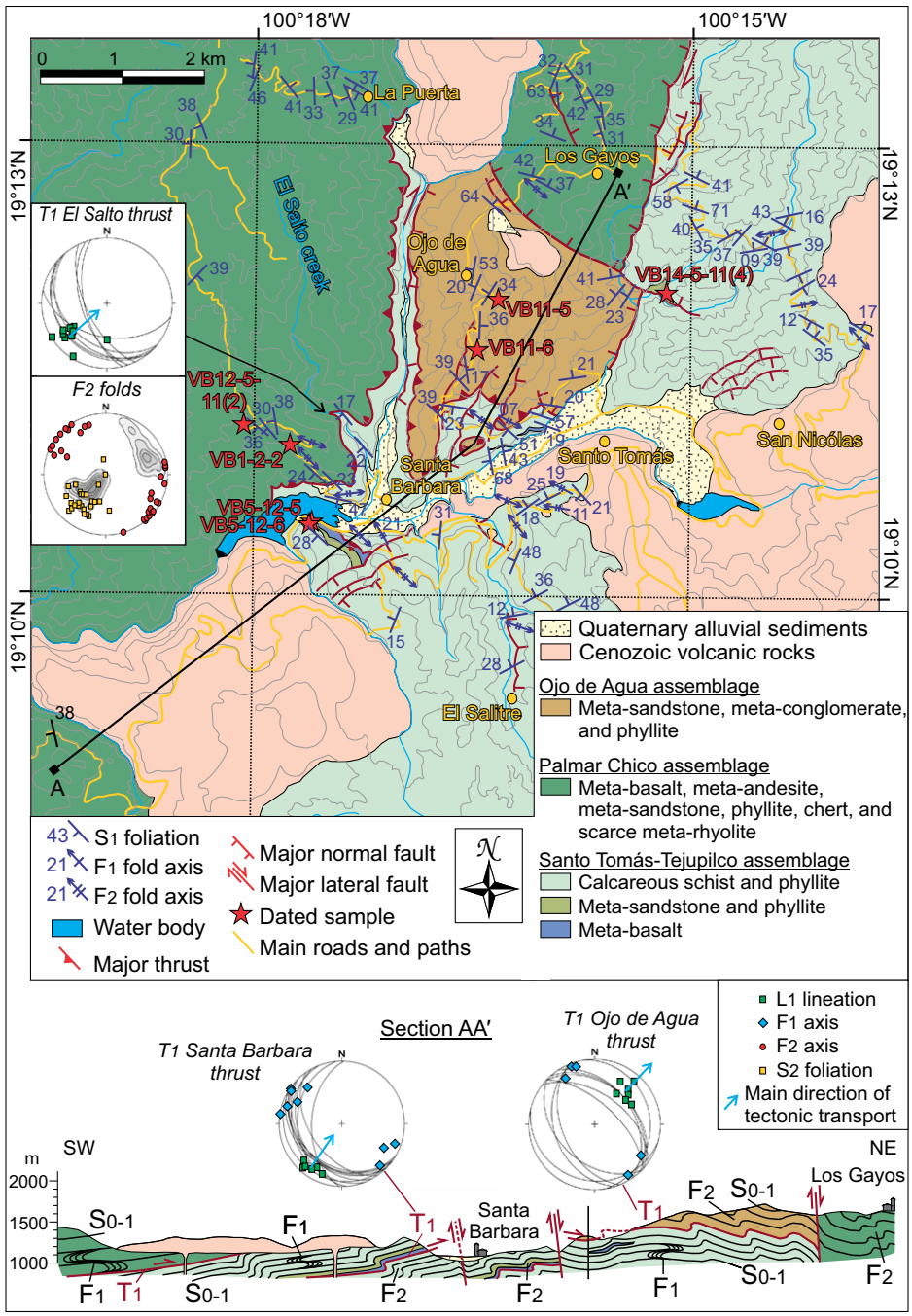

Figure 4. Detailed geologic map and section showing the distribution of the different units exposed in the Santo Tomás area, as well as the extension and kinematics of the major tectonic structures.

At least two superposed shortening phases can be recognized in rocks of the Santo Tomás–Tejupilco assemblage, confirming the general structural evolution proposed by Fitz-Díaz et al. (2008). The D_1 deformation phase is expressed by NW-SE–striking, top-to-the-NE T_1 ductile shear zones and F_1 isoclinal folds with NW-SE–striking, horizontal to gently NW-plunging axes (Fig. 4). The D_2 phase is represented by NW-SE–striking, top-to-the-SW T_2 brittle to brittle-ductile shear zones and F_2 open to isoclinal folds with NW-SE–striking, subhorizontal axes that are superposed to D_1 structures (Fig. 4). Consid-

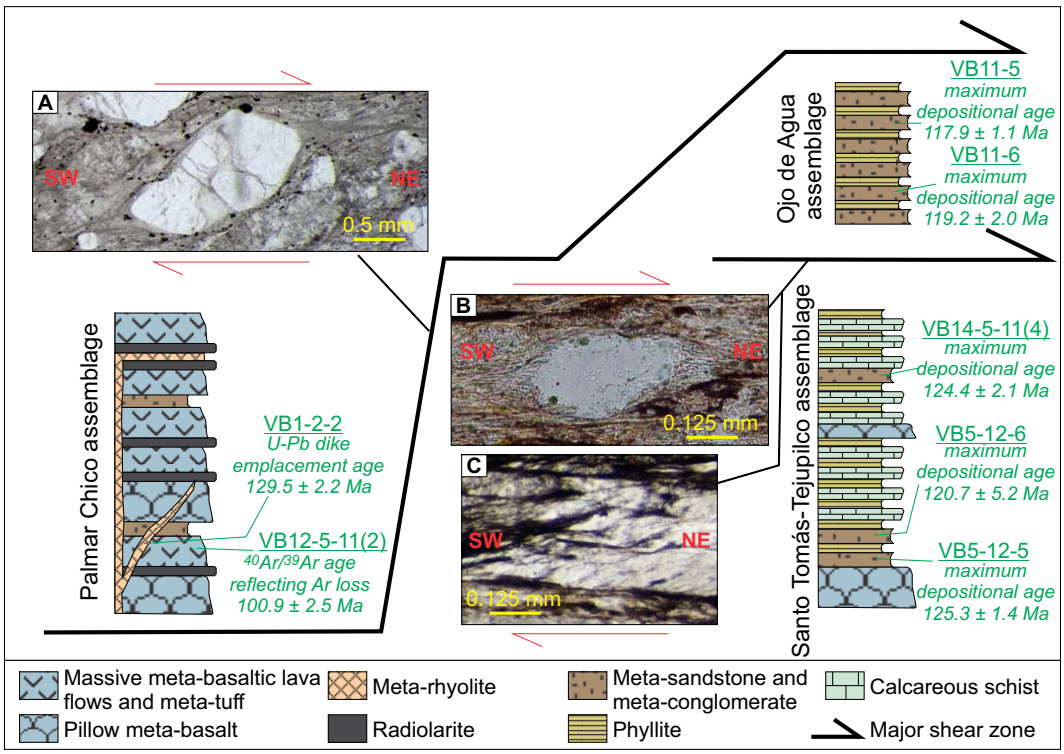

Figure 5. Tectono-stratigraphic framework of the different assemblages recognized in the Santo Tomás area. Photomicrographs indicating the kinematics of the major zones are presented: (A and B) sigma-porphyroclast; and (C) S-C structures observed on cuts parallel to the XZ-plane of the finite ellipsoids indicate a top-to-the-NE direction of tectonic transport.

ering the strong deformation affecting the Santo Tomás–Tejupilco assemblage, it is impossible to estimate a reliable stratigraphic thickness for this succession.

In the western part of the study area, the Santo Tomás–Tejupilco assemblage is tectonically overlain by the Palmar Chico assemblage along a kilometer-scale, top-to-the-NE T_1 shear zone (Figs. 4 and 5A). The Palmar Chico assemblage is composed of a low-grade greenschist-facies, submarine arc succession made up of pillow and massive metabasalt, hyaloclastite, basaltic metatuff, meta-andesite, black chert, metamorphosed epiclastic rocks, and scarce metarhyolitic dikes and flows (Fig. 5). Metarhyolitic dikes are well exposed 1 km NW of the village of Santa Barbara (Fig. 4). These dikes cut metasandstone, phyllite, and metatuff of the Palmar Chico assemblage and locally display fluidal peperites along their contacts (Figs. 6A and 6B). Rhyolitic metatuff layers are interbedded with metasandstone and radiolarite of the Palmar Chico assemblage 1.5 km W of the village of La Puerta (Fig. 6C). These metarhyolitic tuffs and dikes indicate that scarce felsic volcanic activity was locally contemporaneous with the emplacement of mafic flows of the Palmar Chico assemblage.

At least two main shortening phases can be recognized in the succession of the Palmar Chico assemblage. Similar to the Santo Tomás–Tejupilco assemblage, the D_1 shortening event is represented by NW-SE–striking, top-to-the-NE T_1 shear zones and F_1 isoclinal folds with an S_1 axial plane foliation, whereas the D_2 event is expressed by brittle to brittle-ductile, top-to-the-SW T_2 shear zones and F_2 open to isoclinal folds associated to an S_2 crenulation cleavage (Fig. 4).

In the central part of the study area, the Ojo de Agua assemblage is tectonically sandwiched between the Santo Tomás–Tejupilco and Palmar Chico assemblages (Figs. 4 and 5). The Ojo de Agua assemblage consists of low-grade, greenschist-facies metasandstone, metaconglomerate, and phyllite that display a structural pattern analogous to the one described for the Santo Tomás–Tejupilco and Palmar Chico assemblages. The lower tectonic boundary of the Ojo de Agua assemblage is a NW-SE–striking, top-to-the-NE, ductile T_1 shear zone associated to isoclinal F_1 folds and an S_1 axial plane foliation (Figs. 4, 5B, and 5C). NW-SE–striking, top-to-the-SW T_2 shear zones and open to isoclinal F_2 folds with an S_2 axial plane crenulation cleavage are superposed over previous D_1 structures.

METASANDSTONE PETROGRAPHY

Ten, five, and twelve sections of medium- to coarse-grained metasandstones representative of the Santo Tomás–Tejupilco, Palmar Chico, and Ojo de Agua assemblages, respectively, were selected for modal analysis. The low number of sections selected from the Palmar Chico assemblage results from the pervasive weathering of mafic volcanic and volcaniclastic rocks in the study area, which affects the sampling of representative metasandstones suitable for modal analysis. In order to minimize the effect of pressure-solution and metamorphic crystallization, selected samples are from the least deformed and least recrystallized strata that acted as competent layers during the deformation. Five hundred points were counted for each sample using the Gazzi-Dickinson method (Gazzi, 1966; Dickinson, 1970) and the 0% cutoff proposed by Ingersoll et al. (1984) for the poly-crystalline quartz grains. Grain parameters (Dickinson, 1970; Zuffa, 1985; Critelli et al., 1997) are defined in Table 1, whereas raw and recalculated point-count data are presented in Table 2.

Santo Tomás–Tejupilco Assemblage

Metasandstones from the Santo Tomás–Tejupilco assemblage are metalitharenites and metafeldspathic litharenites (Fig. 7A). They are composed of ubiquitous monocrystalline quartz (37%–61% of the total counted grains), lithic fragments (15%–38%), feldspar (6%–17%, plagioclase/total feldspar ratio (P/F) = 25%–41%), polycrystalline quartz (2%–11%), and subordinate dense minerals (<1%) (Figs. 7B and 7C). Lithics are volcanic and low-grade metasedimentary fragments (Fig. 7D). Volcanic grains

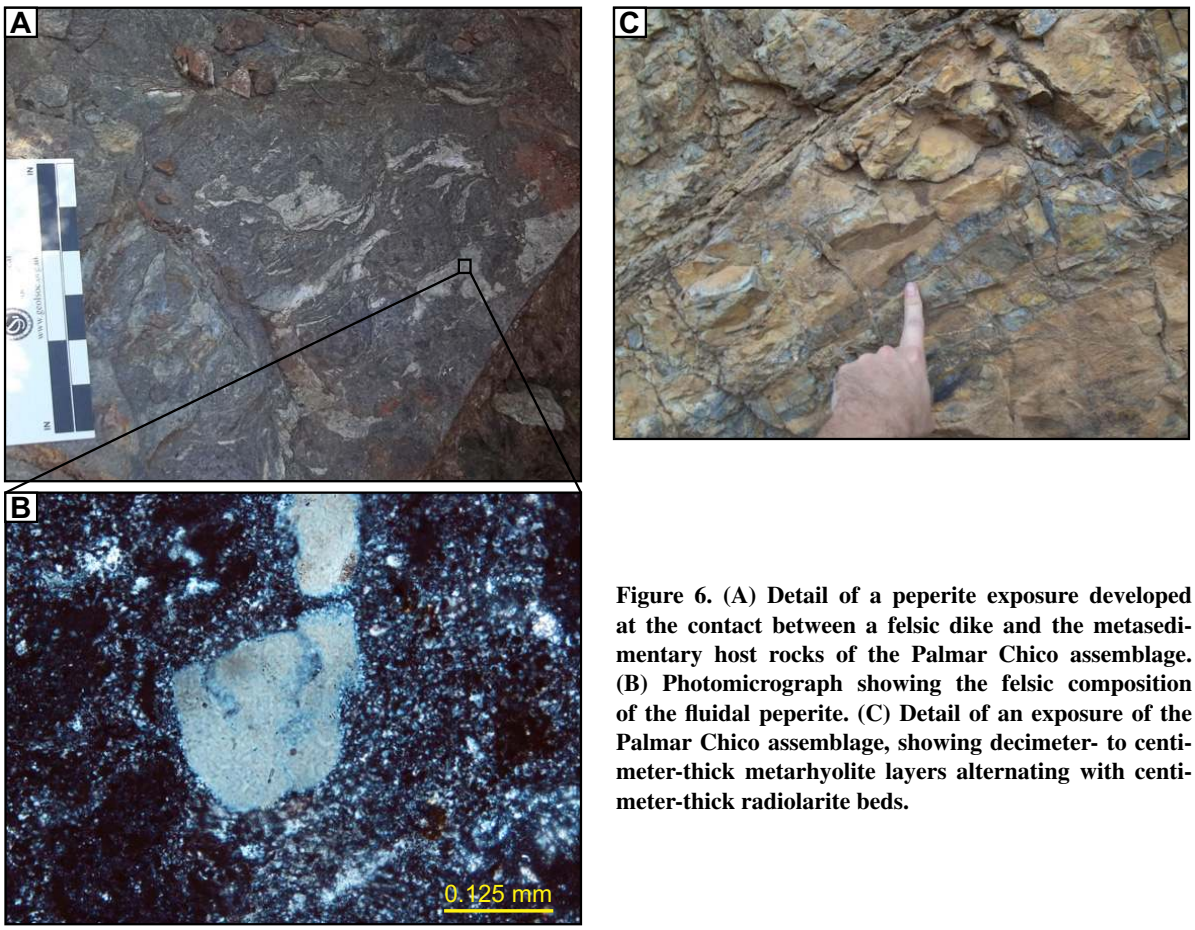

Figure 6. (A) Detail of a peperite exposure developed at the contact between a felsic dike and the metasedimentary host rocks of the Palmar Chico assemblage. (B) Photomicrograph showing the felsic composition of the fluidal peperite. (C) Detail of an exposure of the Palmar Chico assemblage, showing decimeter- to centimeter-thick metarhyolite layers alternating with centimeter-thick radiolarite beds.

are exclusively porphyritic, granular to seriate, felsic fragments (Fig. 7E), and are composed of quartz, K-feldspar, and minor plagioclase phenocrysts in a dominantly quartz-feldspathic groundmass (Fig. 8A). Metasedimentary grains are moderately to well-foliated quartz-sericite to quartz-muscovite metasiltstone and phyllite (Fig. 8B).

Palmar Chico Assemblage

Metasandstones from the Palmar Chico assemblage are metalithic arkoses and metafeldspathic litharenites (Fig. 7A). These rocks are characterized by very low amounts of monocrystalline (0%–2%) and polycrystalline quartz (2%–5%) and high abundances of feldspar (45%–54%, P/F = 98%–100%) and volcanic fragments (33%–46%) (Figs. 7B–7D). The latter are almost exclusively mafic to intermediate, lathwork to microlitic grains (Fig. 7E). Lathwork volcanic grains are composed of sand-sized plagioclase phenocrysts in a groundmass of interstitial dark-brown volcanic glass and opaque minerals (Fig. 8C). Pyroxene phenocrysts are scarce and pervasively oxidized. Microlitic grains contain dark-brown volcanic glass and variable amounts of plagioclase, opaque minerals, and very scarce pyroxene microlites, which are <0.0625 mm long and are visible at high magnification (Fig. 8D). Subordinate felsic volcanic grains (0%–2%) are composed of quartz and feldspar phenocrysts in a quartz-feldspathic groundmass.

Ojo de Agua Assemblage

Metasandstones from the Ojo de Agua assemblage are dominantly metafeldspathic litharenites, with minor metalitharenites and metalithic arkoses (Fig. 7A). These rocks contain a wider variety of framework grains relative to the other assemblages exposed in the

TABLE 1. KEY INDICES FOR FRAMEWORK COMPOSITION AND RATIO PARAMETERS USED FOR METASANDSTONES OF THE SANTO TOMÁS

Key indices	Definition
Qm	Monocrystalline quartz
Qp	Polycrystalline quartz according to the 0% cutoff of Ingersoll et al. (1984)
Qt	Total quartz (Qm + Qp)
K	Potassium feldspar
P	Plagioclase
F	Total feldspar (K + P)
P/F	Plagioclase/total feldspar ratio
Lvl	Lathwork volcanic grain
Lvmi	Microlitic volcanic grain
Lvf	Felsic volcanic and metavolcanic grains
Lvm	Total volcanic and metavolcanic grains (Lvl + Lvmi + Lvf)
Lsm	Sedimentary and low-grade metasedimentary siliciclastic grains
CE	Extrabasinal calcareous grain
L	Total lithic grains (Lvm + Lsm + CE)
Micro	Microgranular grain
Dense	Dense minerals
Misc	Matrix + diagenetic, and postdiagenetic components

study area. In order of abundance they are composed of: monocrystalline quartz (30%–49%), volcanic and metavolcanic grains (18%–31%), feldspar (10%–25%, P/F = 26%–76%), polycrystalline quartz (4%–10%), metasedimentary siliciclastic fragments (1%–7%), extrabasinal carbonate (1%–4%), and subordinate microgranular grains and dense minerals (<1.2%) (Figs. 7B–7D). Volcanic and metavolcanic fragments vary from mafic to felsic and are the most abundant lithic grains in the Ojo de Agua metasandstones (Fig. 7D). Felsic grains are composed of quartz, K-feldspar, and minor plagioclase phenocrysts in a quartz-feldspathic groundmass. Some of these grains display a penetrative foliation defined by fine-grained sericite (Fig. 8E). Mafic volcanic grains vary from lathwork to microlitic, with a slight predominance of the lathwork type in most samples. Metasedimentary fragments also occur in all analyzed samples and can be distinguished into siliciclastic and calcareous types. Siliciclastic grains are represented by well- to slightly foliated quartz-sericite and quartz-muscovite metasiltstones and scarce phyllite. Calcareous fragments were observed only in four of the point-counted samples. They vary from nonfoliated, slightly recrystallized micrite to pervasively foliated and recrystallized calcareous grains (Fig. 8F).

U-Pb GEOCHRONOLOGY

In order to constrain the provenance and maximum depositional age of the assemblages exposed in the Santo Tomás area, zircons separated from five metasandstones and one metarhyolite were dated by laser ablation inductively-coupled plasma mass spectrometry (LA-ICPMS) at the Laboratorio de Estudios Isotópicos of Centro de Geociencias, Universidad Nacional Autónoma de México. Details of the analytical data are given in Table A in the Supplemental File[1], whereas a synthesis of the results is presented in Table 3. Tera and Wasserburg (1972) concordia, weighted mean, and probability density plots (Figs. 9 and 10) were obtained using Isoplot v.3.06 (Ludwig, 2004). Plots were constructed using the $^{206}Pb/^{238}U$ age for zircons younger than 1.0 Ga, whereas grains older than 1.0 Ga were quoted using their $^{207}Pb/^{206}Pb$ ages. As a statistical rejection criterion, 10% normal and 5% reverse discordancy was chosen (Harris et al., 2004; Gehrels,

[1]Supplemental File. U-Pb and $^{40}Ar/^{39}Ar$ geochronologic data. If you are viewing the PDF of this paper or reading it offline, please visit http://dx.doi.org/10.1130/GES01055.S1 or the full-text article on www.gsapubs.org to view the Supplemental File.

TABLE 2. POINT-COUNTING RAW DATA AND RECALCULATED PARAMETERS FOR METASANDSTONES OF THE SANTO TOMÁS AREA

	Point-counting proportions											
Sample	Qm	Qp	K	P	Lvl	Lvmi	Lvf	Lsm	CE	Micro	Dense	Misc	TOT
Santo Tomás–Tejupilco assemblage													
ST16-5-11(8)a	190	34	37	26	0	0	118	31	0	11	5	48	500
ST16-5-11(8)b	247	53	38	13	0	0	81	22	0	0	77	39	500
VB5-12-5A	194	9	55	24	0	0	152	10	0	5	3	48	500
VB5-12-5B	183	28	56	27	0	0	133	15	0	7	7	44	500
VB5-12-5C	183	14	36	16	0	0	167	24	0	0	4	56	500
ST15-5-11(7)	224	24	50	26	0	0	104	15	0	4	2	51	500
VB5-12-6	219	34	53	20	0	0	95	31	0	0	2	46	500
VB14-5-11(3)	260	37	29	15	0	0	50	49	0	0	5	55	500
VB14-5-11(4)b	303	42	20	9	0	0	41	41	0	0	2	42	500
VB14-5-11(4)c	294	38	25	11	0	0	40	37	0	2	1	52	500
Palmar Chico assemblage													
VB2-10-4	12	27	5	223	103	72	11	0	0	0	3	44	500
VB2-10-3	0	15	0	271	91	73	0	0	0	0	7	43	500
VB2-10-2	9	21	0	242	121	68	2	0	0	0	5	32	500
ST16-5-11(2)	0	10	0	223	137	94	0	0	0	0	1	35	500
ST16-5-11(4)	2	15	1	257	107	83	5	0	0	0	2	28	500
Ojo de Agua assemblage													
ST18-5-11(1)a	246	48	27	34	37	9	63	11	0	0	3	22	500
ST18-5-11(1)b	229	39	69	24	30	15	47	14	0	0	2	31	500
ST18-5-11(1)c	171	21	75	50	32	11	63	3	0	0	0	74	500
ST18-5-11(1)d	190	27	58	43	23	7	86	7	0	0	4	55	500
VB11-5b	176	33	45	22	17	11	129	19	0	0	3	45	500
VB14-5-11-11(6)b	212	24	16	36	49	26	47	32	10	0	3	45	500
VB5-12-9b	193	18	40	37	32	9	75	35	21	6	3	31	500
VB5-12-12a	170	48	50	57	30	13	72	12	0	3	3	42	500
VB5-12-12b	188	22	54	40	35	10	81	24	9	0	2	35	500
VB5-12-12c	201	32	37	35	29	13	93	22	5	0	2	31	500
ST17-5-11(1)	161	37	34	86	52	27	41	16	0	0	3	43	500
VB11-6	152	28	30	93	61	20	54	11	0	0	1	50	500

(*continued*)

TABLE 2. POINT-COUNTING RAW DATA AND RECALCULATED PARAMETERS FOR METASANDSTONES OF THE SANTO TOMÁS AREA (*continued*)

	Recalculated parameters											
Sample	QmFL%Qm	QmFL%F	QmFL%L	QtFL%Qt	QtFL%F	QtFL%L	QpLvm (Lsm + CE) %Qp	QpLvm (Lsm + CE) %Lvm	QpLvm (Lsm + CE)% (Lsm + CE)	(Lsm + CE)Lvf (Lvl + Lvmi)% (Lsm + CE)	(Lsm + CE)Lvf (Lvl + Lvmi)%Lvf	(Lsm + CE)Lvf (Lvl + Lvmi) %(Lvf + Lvmi)	P/F
Santo Tomás–Tejupilco assemblage													
ST16-5-11(8)a	43.6	14.4	42.0	51.4	14.4	34.2	18.6	64.5	16.9	20.8	79.2	0.0	41.3
ST16-5-11(8)b	54.4	11.2	34.4	66.1	11.2	22.7	34.0	51.9	14.1	21.4	78.6	0.0	25.5
VB5-12-5A	43.7	17.8	38.5	45.7	17.8	36.5	5.3	88.9	5.8	6.2	93.8	0.0	30.4
VB5-12-5B	41.4	18.8	39.8	47.7	18.8	33.5	15.9	75.6	8.5	10.1	89.9	0.0	32.5
VB5-12-5C	41.6	11.8	46.6	44.8	11.8	43.4	6.8	81.5	11.7	12.6	87.4	0.0	30.8
ST15-5-11(7)	50.6	17.2	32.3	56.0	17.2	26.9	16.8	72.7	10.5	12.6	87.4	0.0	34.2
VB5-12-6	48.5	16.2	35.4	56.0	16.2	27.9	21.3	59.4	19.4	24.6	75.4	0.0	27.4
VB14-5-11(3)	59.1	10.0	30.9	67.5	10.0	22.5	27.2	36.8	36.0	49.5	50.5	0.0	34.1
VB14-5-11(4)b	66.4	6.4	27.2	75.7	6.4	18.0	33.9	33.1	33.1	50.0	50.0	0.0	31.0
VB14-5-11(4)c	66.1	8.1	25.8	74.6	8.1	17.3	33.0	34.8	32.2	48.1	51.9	0.0	30.6
Palmar Chico assemblage													
VB2-10-4	2.6	50.3	47.0	8.6	50.3	41.1	12.7	87.3	0.0	0.0	5.9	94.1	97.8
VB2-10-3	0.0	60.2	39.8	3.3	60.2	36.4	8.4	91.6	0.0	0.0	0.0	100.0	100.0
VB2-10-2	1.9	52.3	45.8	6.5	52.3	41.3	9.9	30.1	0.0	0.0	1.0	99.0	100.0
ST16-5-11(2)	0.0	48.1	51.9	2.2	48.1	49.8	4.1	65.9	0.0	0.0	0.0	100.0	100.0
ST16-5-11(4)	0.4	54.9	44.7	3.6	54.9	41.5	7.1	92.9	0.0	0.0	2.6	97.4	99.6
Ojo de Agua assemblage													
ST18-5-11(1)a	51.8	12.8	35.36842	61.9	12.8	25.3	28.6	64.9	6.5	9.2	52.5	38.3	55.7
ST18-5-11(1)b	49.0	19.9	31.04925	57.4	19.9	22.7	26.9	63.4	9.7	13.2	44.3	42.5	25.8
ST18-5-11(1)c	40.1	29.3	30.51643	45.1	29.3	25.6	16.2	81.5	2.3	2.8	57.8	39.4	40.0
ST18-5-11(1)d	43.1	22.9	34.01361	49.2	22.9	27.9	18.0	77.3	4.7	5.7	69.9	24.4	42.6
VB11-5b	38.9	14.8	46.23894	46.2	14.8	38.9	15.8	75.1	9.1	10.8	73.3	15.9	32.8
VB14-5-11(6)b	46.9	11.5	41.59292	52.2	11.5	36.3	12.8	64.9	22.3	25.6	28.7	45.7	69.2
VB11-6	42.0	16.7	41.30435	45.9	16.7	37.4	9.5	61.1	29.5	32.6	43.6	23.8	48.1
VB5-12-12a	37.6	23.7	38.71681	48.2	23.7	28.1	27.4	65.7	6.9	9.4	56.7	33.9	53.3
VB5-12-12b	40.6	20.3	39.09287	45.4	20.3	34.3	12.2	69.6	18.2	20.8	50.9	28.3	42.6
VB5-12-12c	43.0	15.4	41.54176	49.9	15.4	34.7	16.5	69.6	13.9	16.7	57.4	25.9	48.6
ST17-5-11(1)	35.5	26.4	38.10573	43.6	26.4	30.0	21.4	69.4	9.2	11.8	30.1	58.1	71.7
VB5-12-9b	33.9	27.4	38.75278	40.1	27.4	32.5	16.1	77.6	6.3	7.5	37.0	55.5	75.6

Note: Abbreviations are defined in Table 1.

2011), and none of these zircons are included in the plots and discussion below. The maximum depositional robust age (MDRA) of each assemblage is constrained by the weighted mean of the youngest cluster defined by at least three zircon grains overlapping in age at 2σ (Gehrels et al., 2006).

Santo Tomás–Tejupilco Assemblage

Sample VB14-5-11(4) is a metasublitharenite collected from the eastern part of the study area, 1.5 km NW of the village of San Nicolas (Figs. 4 and 5). This sample yielded abundant colorless and pink detrital zircons ranging from 30 to 180 μm in size. Cathodoluminescence images show the predominance of concentric oscillatory and sector zoning that are typical of magmatic zircons (Connelly, 2001; Corfu et al., 2003). Th/U ratios are >0.1 for all but three crystals, supporting a magmatic origin for at least the great majority of these zircons (Rubatto, 2002). Seventy-five magmatic zircons yielded concordant to slightly discordant ages that range from ca. 1510 to ca. 120 Ma (Fig. 9). Forty-three percent of these zircons yielded Mesoproterozoic to Late Triassic ages, with great dominance of Grenvillian, Pan-African, and Silurian–Permian grain populations (Fig. 10). Twenty-one percent of analyzed zircons returned Early and Middle Jurassic ages ranging from 201 to 172 Ma. Finally, 26% of total grains yielded Late Jurassic to Early Cretaceous ages that span between ca. 158 to ca. 120 Ma (Fig. 10). A MDRA of 124.4 ± 2.1 Ma for the Santo Tomás–Tejupilco assemblage is obtained from sample VB14-5-11(4) (Fig. 9 and Table 3).

Samples VB5-12-5 and VB5-12-6 are metafeldspathic litharenite collected from two contiguous beds in the western part of the study area (Figs. 4 and 5). These samples yielded abundant colorless, amber, and pinkish zircons that vary in size from 40 to 230 μm. Almost all grains show oscillatory and sector zoning locally developed around low-luminescent xenocrystic cores. Th/U ratios are >0.1 for all but one crystal. Both samples contain zircon populations similar to the ones documented for sample VB14-5-11(4), even though in different proportions. In fact, Upper Jurassic–Lower Cretaceous zircons represent the great majority of the analyzed grains in samples VB5-12-5 and VB5-12-6, with abundances of 98% and 79%, respectively (Figs. 9 and 10). Subordinate Middle Jurassic grains are also present in both samples, whereas early Paleoproterozoic, Grenvillian, Pan-African, Permian, and Late Triassic populations are contained exclusively in sample VB5-12-6 (Figs. 9 and 10). Samples

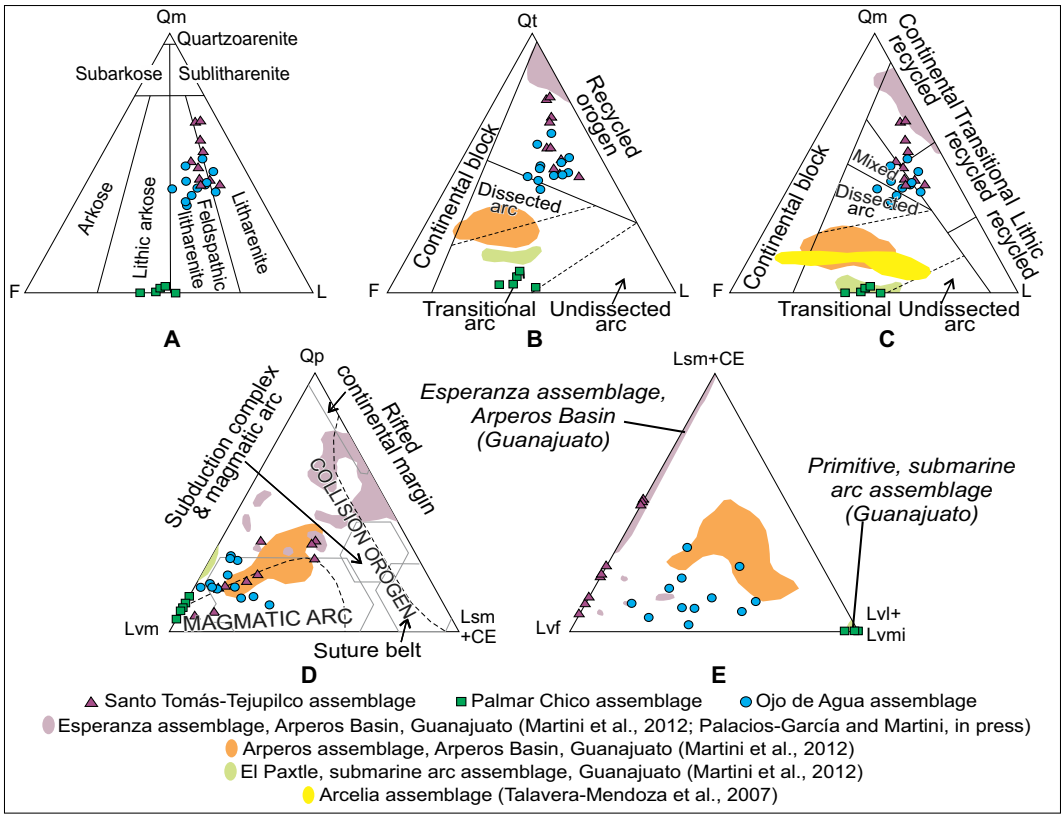

Figure 7. (A) QFL, (B) QtFL, (C) QmFL, (D) QpLvm(Lsm + CE), and (E) (Lsm + CE) Lvf(Lvl + Lvmi) diagrams showing the distinct composition of sandstones from the Ojo de Agua, Palmar Chico, and Santo Tomás–Tejupilco assemblages. Composition and provenance of the analyzed sandstone are discussed in the text. Compositional fields in (A) are from Folk (1974). Provenance fields are from Dickinson (1985) for (B) and (C). Dashed-line fields in (D) are from Dickinson and Suczek (1979), while solid lines are from Ingersoll and Suczek (1979).

VB5-12-5 and VB5-12-6 define MDRAs of 125.3 ± 1.4 and 120.7 ± 5.2 Ma, respectively, for the Santo Tomás–Tejupilco assemblages (Fig. 9 and Table 3). These ages are statistically undistinguishable within errors and overlap with the MDRA obtained from sample VB14-5-11(4).

Palmar Chico Assemblage

Sample VB1-2-2 is a metarhyolite collected from a dike with peperites cutting the mafic volcaniclastic succession of the Palmar Chico assemblage (Figs. 4 and 5). This sample yielded a few colorless and amber euhedral zircons that vary in size from 20 to 170 µm. Cathodoluminescence images of these crystals show oscillatory zoning, locally developed around low-luminescent xenocrystic cores. Th/U ratios are >0.1 for all but one grain. Given the small dimension of most grains and the recurrent apatite and opaque inclusions, only 17 crystals returned acceptable ages that vary from 1253 to 126 Ma (Fig. 9). Nine zircon grains yielded ages between 135 and 126 Ma, which define a $^{206}Pb/^{238}U$ weighted mean of 129.5 ± 2.2 Ma (Fig. 9 and Table 3). This age is interpreted to reflect the time of emplacement of this metarhyolitic dike. Concordant to slightly discordant ages between 1253 and 347 Ma were obtained from seven zircon grains (Fig. 9), and these ages are interpreted to represent xenocrysts inherited from the Palmar Chico arc basement, which is possibly represented by Upper Triassic turbidites of the Arteaga Complex.

Ojo de Agua Assemblage

Samples VB11-5 and VB11-6 are metalitharenites collected from the Ojo de Agua assemblage (Figs. 4 and 5). These samples yielded abundant colorless and pink zircons that vary in size from 60 to 250 µm. Cathodoluminescence images show the predominance of concentric oscillatory zoning. Th/U ratios are >0.1 for all but five grains. Similar zircon populations are present in the two samples (Figs. 9 and 10). The most representative population is composed of Upper Jurassic–Lower Cretaceous (ca. 159–113 Ma) zircons, which represent the 84% and 73% of the total analyzed grains for sample VB11-5 and VB11-6, respectively (Fig. 9B). Only 1%–3% of the total grains yielded Middle Jurassic ages (ca. 170–163 Ma), whereas Neoarchean, Paleoproterozoic, Grenvillian, Pan-African, and Ordovician zircons display abundances in the range of 14% and 24%. Samples VB11-5 and VB11-6 define MDRAs of 117.9 ± 1.1 and 119.2 ± 2.0 Ma, respectively, for the Ojo de Agua assemblage (Fig. 9 and Table 3). These ages are equivalent within errors.

^{40}Ar-^{39}Ar GEOCHRONOLOGY

Sample VB12-5-11(2) is a metabasalt collected from the Palmar Chico assemblage (Figs. 4 and 5). A plagioclase concentrate from this sample was prepared and dated by the ^{40}Ar-^{39}Ar method at the Laboratorio de Geocronología of Centro de Investigación Científica y Educación Superior de Ensenada. Results are presented in Figures 11A–11C, whereas details of the analytical data and methodology are given in Table B in the Supplemental File (see footnote 1). Two laser step-heating experiments were performed, and reproducible age spectra were obtained (Fig. 11A). Due to the low potassium content in the analyzed plagioclase, the age results display big uncertainties. A 101.6 ± 2.4 Ma plateau age was obtained for the last four fractions of the second experiment, which represent 80.40% of the ^{39}Ar released. The mean square of weighted deviates for the plateau segment is 1.1, which indicates that the plateau age includes the goodness of fit and the uncertainty in the J parameter. Data of the two experiments were combined in the $^{36}Ar/^{40}Ar$ versus $^{39}Ar/^{40}Ar$ correlation diagram (Fig. 11C), where they align to define an isochron age of 100.9 ± 2.5 Ma. Considering that the analyzed basaltic flow is cut by the 129.5 ± 2.2 Ma metarhyolitic dike (sample VB1-2-2), we interpret that the 100.9 ± 2.5 Ma

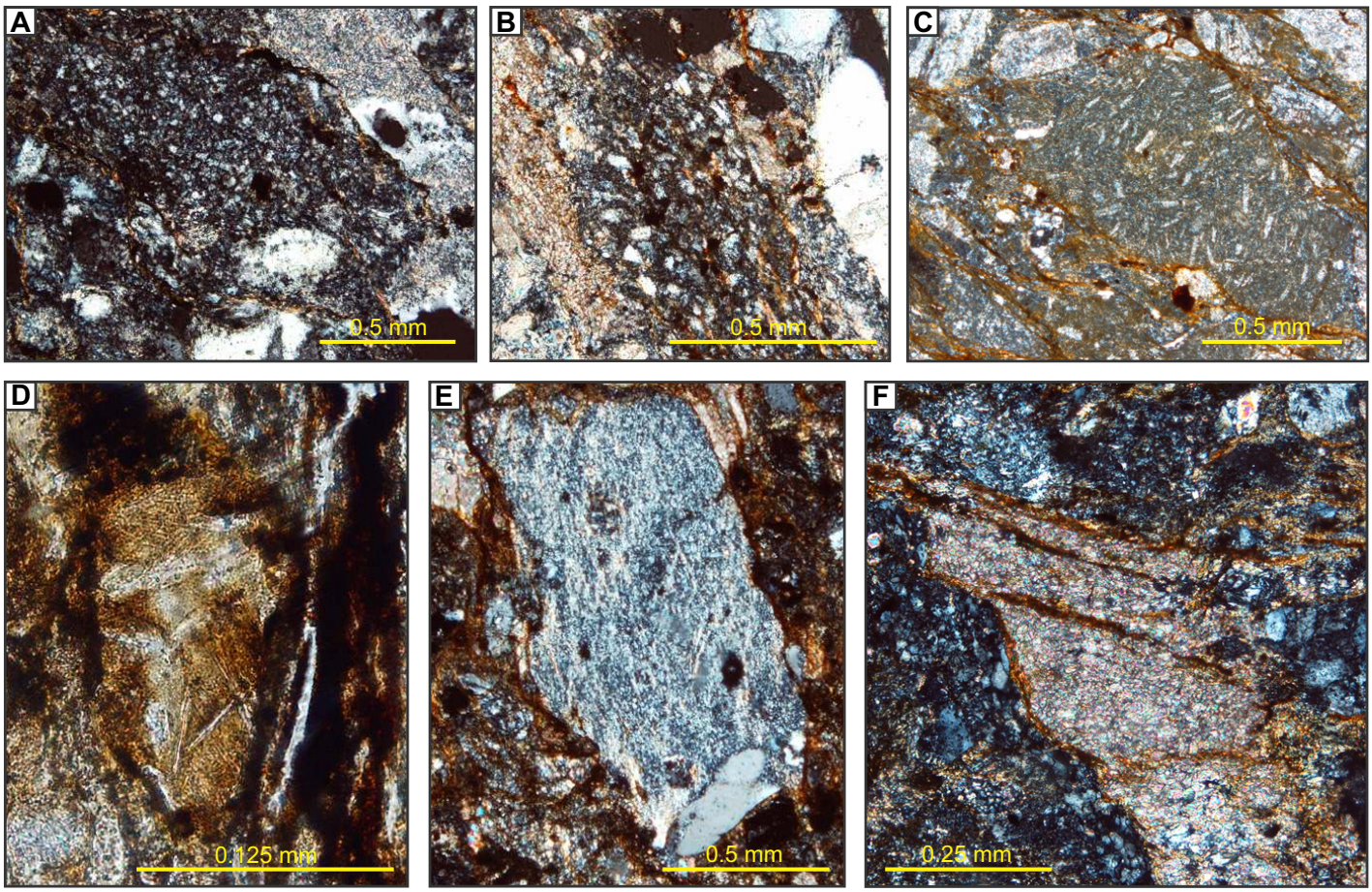

Figure 8. Photomicrographs showing details of: (A) a felsic volcanic grain and (B) a quartz-rich metasiltite fragment from metasandstones of the Santo Tomás–Tejupilco assemblage; (C) lathwork and (D) microlitic volcanic grains from metasandstones of the Palmar Chico assemblage; (E) a foliated felsic metavolcanic grain, and (F) a foliated extrabasinal calcareous fragment from metasandstones of the Ojo de Agua assemblage.

^{40}Ar-^{39}Ar age better reflects Ar loss and partial or total resetting rather than the time of the flow emplacement (Table 3). This is also confirmed by the age spectrum that suggests some thermal disturbance after rock formation (Fig. 11A).

METASANDSTONE PROVENANCE

Santo Tomás–Tejupilco Assemblage

Metasandstones from the Santo Tomás–Tejupilco assemblage are characterized by high percentages of monocrystalline quartz, moderate to low amounts of felsic volcanic fragments and feldspar, and by the lack of mafic and intermediate volcanic grains with lathwork and microlitic textures (Figs. 7B–7E). These compositional attributes discard the dominantly mafic to intermediate arc assemblages of the Guerrero terrane as possible sources for metasandstones of the Santo Tomás–Tejupilco assemblage. Moreover, the high percentage of monocrystalline quartz in metasandstones from the Santo Tomás–Tejupilco assemblage cannot be easily explained assuming a Guerrero terrane provenance. In fact, the only quartz-rich sources within the Guerrero terrane are Upper Triassic metaturbidites of the Arteaga Complex (Centeno-García et al., 2003), which were widely covered by the arc assemblages during the Late Jurassic and Early Cretaceous (Centeno-García et al., 2008). Based on these considerations, a provenance from the North American continental mainland is envisaged. Such hypothesis is confirmed by the occurrence of Lower Jurassic zircons in metasandstones from the Santo Tomás–Tejupilco assemblage. In fact, Lower Jurassic igneous rocks are presently unknown within the Guerrero terrane, whereas they are well exposed in the North American continental mainland and are represented by the dominantly felsic Nazas volcanic province (Bartolini and Spell, 1997; Barboza-Gudiño et al., 2008; Rubio-Cisneros and Lawton, 2011).

Considering a North American mainland provenance for the Santo Tomás–Tejupilco assemblage, the ca. 120–158 zircon grains in the analyzed metasandstones were likely derived from the Upper Jurassic–Lower Cretaceous rhyodacitic dikes and lava flows that locally fringe the western margin of nuclear Mexico at Actopan and Taxco (Campa-Uranga et al., 2012; Abascal and Murillo-Muñetón, 2013) (Fig. 1). Moreover, pre-Jurassic metaigneous and metasedimentary rocks of the North American mainland ubiquitously contain lower Mesoproterozoic, Grenvillian, Pan-African, Silurian–Ordovician, and Permian–Triassic zircons populations (Centeno-García, 2005; Barboza-Gudiño et al., 2010; Ortega-Flores et al., 2014) and, therefore, may represent possible sources for the Mesoproterozoic–Triassic zircon grains contained in metasandstones of the Santo Tomás–Tejupilco assemblage.

TABLE 3. SUMMARY OF THE U-Pb AND $^{40}Ar/^{40}Ar$ RESULTS

Sample	Latitude (°N)	Longitude (°W)	Tectonostratigraphic unit	Rock type	Age (Ma)	Method	Material dated	Interpretation
VB14-5-11(4)	19°12′01.09″	100°15′14.18″	Santo Tomás–Tejupilcol assemblage	Metasublitharenite	124.4 ± 2.1	U-Pb	Zircon	Maximum depositional age
VB5-12-5	19°10′28.39″	100°17′39.57″	Santo Tomás–Tejupilcol assemblage	Metafeldspathic litharenite	125.3 ± 1.4	U-Pb	Zircon	Maximum depositional age
VB5-12-6	19°10′28.39″	100°17′39.57″	Santo Tomás–Tejupilcol assemblage	Metafeldspathic litharenite	120.7 ± 5.2	U-Pb	Zircon	Maximum depositional age
VB1-2-2	19°11′01.27″	100°17′51.74″	Palmar Chico assemblage	Metarhyolite (dike)	129.5 ± 2.2	U-Pb	Zircon	Age of dike emplacement
VB12-5-11(2)	19°11′06.84″	100°18′08.72″	Palmar Chico assemblage	Metabasalt (lava flow)	100.9 ± 2.5	$^{40}Ar/^{40}Ar$	Plagioclase	Ar loss
VB11-5	19°11′59.87″	100°16′25.96″	Ojo de Agua assemblage	Metalitharenite	117.9 ± 1.1	U-Pb	Zircon	Maximum depositional age
VB11-6	19°11′39.64″	100°16′33.38″	Ojo de Agua assemblage	Metalitharenite	119.2 ± 2.0	U-Pb	Zircon	Maximum depositional age

Palmar Chico Assemblage

Metasandstones from the Palmar Chico assemblage are dominantly composed of plagioclase and volcanic lithic grains with microlitic and lathwork textures (Figs. 7B–7E). These characteristics are typical of epiclastic deposits of the Guerrero terrane exposed at Guanajuato (Martini et al., 2012) (Figs. 7B–7E) and suggest that metasandstones from the Palmar Chico assemblage were essentially sourced from mafic and intermediate volcanic sources that can be reasonably related to metabasalt and metaandesite, with which they are interbedded.

Ojo de Agua Assemblage

Metasandstones from the Ojo de Agua assemblage are composed of monocrystalline quartz, plagioclase, volcanic lithic grains with microlitic, lathwork, and felsic textures, minor metasedimentary fragments, and extrabasinal carbonates (Figs. 7B–7E). Such a variety of framework components reflects derivation from different sources. Mafic to intermediate volcanic lithic grains with microlitic and lathwork textures are major components only in deposits derived from the Bajocian–Cenomanian arc assemblages of the Guerrero terrane (Talavera-Mendoza et al., 2007; Martini et al., 2011; Martini et al., 2012) (Figs. 7B–7E). The occurrence of ubiquitous Middle Jurassic–Lower Cretaceous zircon grains in metasandstones from the Ojo de Agua assemblage permits a Guerrero terrane provenance. On the other hand, sandstones with percentages of monocrystalline quartz >30% are unusual in deposits derived from the Guerrero terrane, because of the lack of available quartz-rich sources exposed during the Late Jurassic and Early Cretaceous (Centeno-García et al., 2008; Martini et al., 2011). High percentages of monocrystalline quartz generally result from the recycling of quartz-rich metasedimentary and metaigneous rocks of the North American continental mainland (Martini et al., 2011; Palacios-García and Martini, 2014). Contributions from the North American mainland in the metasandstones of the Ojo de Agua assemblage are documented by the presence of sparse Middle Jurassic zircon grains derived from the Nazas volcanic province or Nazas-derived younger deposits. Therefore, the composition of metasandstones from the Ojo de Agua assemblage may result from a mix of sources, which includes the mafic to intermediate arc assemblages of the Guerrero terrane and quartz-rich rocks of nuclear Mexico. Such interpretation implies that by the time of deposition of the Ojo de Agua assemblage, the Guerrero terrane was already juxtaposed to the North American mainland margin, and the interposed Arperos Basin was inverted and exhumed during the collision. Considering that, similarly to the Santo Tomás–Tejupilco and Palmar Chico assemblages, the Ojo de Agua metasandstones are involved in the deformation related to the accretion of the Guerrero terrane, we interpret the Ojo de Agua assemblage as a syntectonic unit deposited during the closure of the Arperos Basin and collision of the arc assemblages to the North American continental mainland. Based on this scenario, the foliated limestone and felsic volcanic grains observed exclusively in metasandstones from the Ojo de Agua assemblage may be derived from the Santo Tomás–Tejupilco succession, which was deposited along the western margin of the North American mainland and subsequently sheared and exhumed during the basin inversion.

RECONSTRUCTING THE ARPEROS BASIN IN SOUTHERN MEXICO

Available paleontologic and geochronologic data constrain the age of the Santo Tomás–Tejupilco assemblage in the Berriasian–Cenomanian (Cantú-Chapa, 1968; Israde-Alcantara and Martínez-Alvarado, 1986; Elías-Herrera et al., 2000; Elías-Herrera et al., 2009; this work) (Fig. 12). Calcareous and siliciclastic metaturbidites of the Santo Tomás–Tejupilco assemblage were previously considered part of the Guerrero terrane (Elías-Herrera et al., 2000; Mendoza and Suástegui, 2000; Centeno-García et al., 2008). However, the provenance analysis presented in this work documents that metasandstones of the Santo Tomás–Tejupilco assemblage were exclusively derived from sources in the North American continental mainland. Based on these considerations, we suggest that the Santo Tomás–Tejupilco assemblage was developed along the North American mainland margin, in a depositional site that was sedimentologically disconnected from the mafic to intermediate volcanic sources of the Guerrero terrane.

At Guanajuato, central Mexico, Tithonian–Aptian, calcareous and siliciclastic metaturbidites with a North American mainland provenance are grouped into the Esperanza assemblage (Fig. 12), which has been interpreted as a submarine fan complex deposited on the eastern margin of the Arperos Basin (Martini et al., 2011; Palacios-García and Martini, 2014). Similarly to the Santo Tomás–Tejupilco assemblage, metasandstones of the Esperanza assemblage are characterized by a high percentage of monocrystalline quartz and low to moderate amounts of feldspar and volcanic lithic grains (Figs. 7B–7E) (Martini et al., 2011; Palacios-García and Martini, 2014). Volcanic grains are

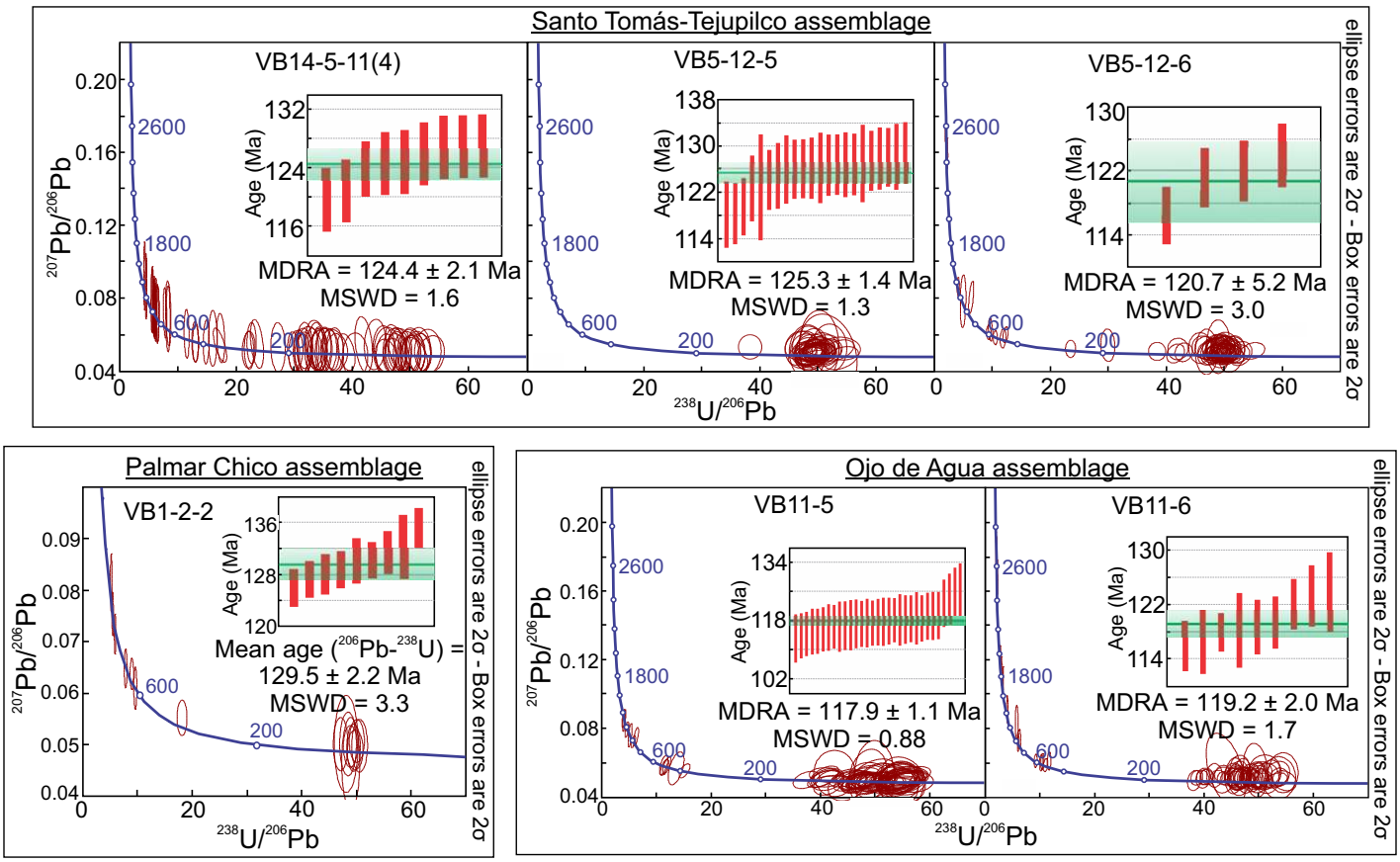

Figure 9. Tera and Wasserburg (1972) diagrams for dated metasandstone samples from the Santo Tomás–Tejupilco, Palmar Chico, and Ojo de Agua assemblages. Plots were constructed using the $^{206}Pb/^{238}U$ age for zircons younger than 1.0 Ga, whereas grains older than 1.0 Ga were quoted using their $^{207}Pb/^{206}Pb$ ages. As a statistical rejection criterion, 10% normal and 5% reverse discordancy were chosen (Harris et al., 2004; Gehrels, 2011), and none of these zircons are included in the plots and discussion below. The maximum depositional robust age (MDRA) of each assemblage is constrained by the weighted mean of the youngest cluster defined by at least three zircon grains overlapping in age at 2σ (Gehrels et al., 2006). MSWD—mean square of weighted deviates.

almost exclusively felsic and suggest a sedimentological disconnection with sources of the Guerrero terrane. Furthermore, as in the Santo Tomás and Tejupilco areas, metaturbidites at Guanajuato are locally interbedded with Upper Jurassic–Lower Cretaceous felsic volcanic rocks and pillow metabasalts (Tardy et al., 1994; Martini et al., 2011; Palacios-García and Martini, 2014). Based on the similar stratigraphy, provenance, and depositional age, we propose a correlation between the Santo Tomás–Tejupilco and Esperanza assemblages and suggest that these assemblages represent turbiditic fans sourced from the North American mainland and deposited along the eastern margin of the Arperos Basin (Figs. 12 and 13A).

At Guanajuato, the western margin of the Arperos Basin is represented by the Arperos assemblage, which is composed of Aptian volcaniclastic metaturbidites derived from the Guerrero terrane interbedded with intraplate-like and MOR basaltic lava flows (Tardy et al., 1994; Martini et al., 2011) (Fig. 12). Similar rocks are not exposed in the study area. However, in the surroundings of Arcelia, ca. 60 km south of Tejupilco (Fig. 3B), Albian–Cenomanian volcaniclastic metaturbidites interbedded with MOR basaltic layers overthrust the Santo Tomás–Tejupilco assemblage with a top-to-the-NE main direction of tectonic transport (Mendoza and Suástegui, 2000; Salinas-Prieto et al., 2000) (Fig. 12). Similarly to metaturbidites of the Arperos assemblage, metasandstones in the Arcelia area were sourced from the Guerrero terrane, and are dominantly composed of plagioclase and mafic to intermediate volcanic lithic grains (Talavera-Mendoza et al., 2007) (Fig. 7C). Moreover, volcaniclastic metaturbidites at Guanajuato and Arcelia contain a similar Upper Jurassic–Lower Cretaceous zircon population (Talavera-Mendoza et al., 2007; Martini et al., 2011), which permits a correlation between the Arperos and Arcelia assemblages (Figs. 12 and 13A).

Based on the proposed correlations, the depositional architecture documented for the Arperos Basin at Guanajuato can be extended in southern Mexico. This scenario confirms the provenance asymmetry previously proposed for the Arperos Basin, which is composed of the North American mainland-sourced Esperanza and Santo Tomás–Tejupilco assemblages on its eastern side and the Guerrero terrane-derived Arperos and Arcelia assemblages on its western side (Figs. 12 and 13A).

A key paleogeographic conflict in reconstructing the Arperos Basin in southern Mexico arises from the multi-arc setting proposed by Talavera-Mendoza et al. (2007). Based on previous $^{40}Ar/^{39}Ar$ ages, these authors argued that the Santo Tomás–Tejupilco and Arcelia assemblages are bounded to the east and west by two distinct arc successions that are the Tithonian–

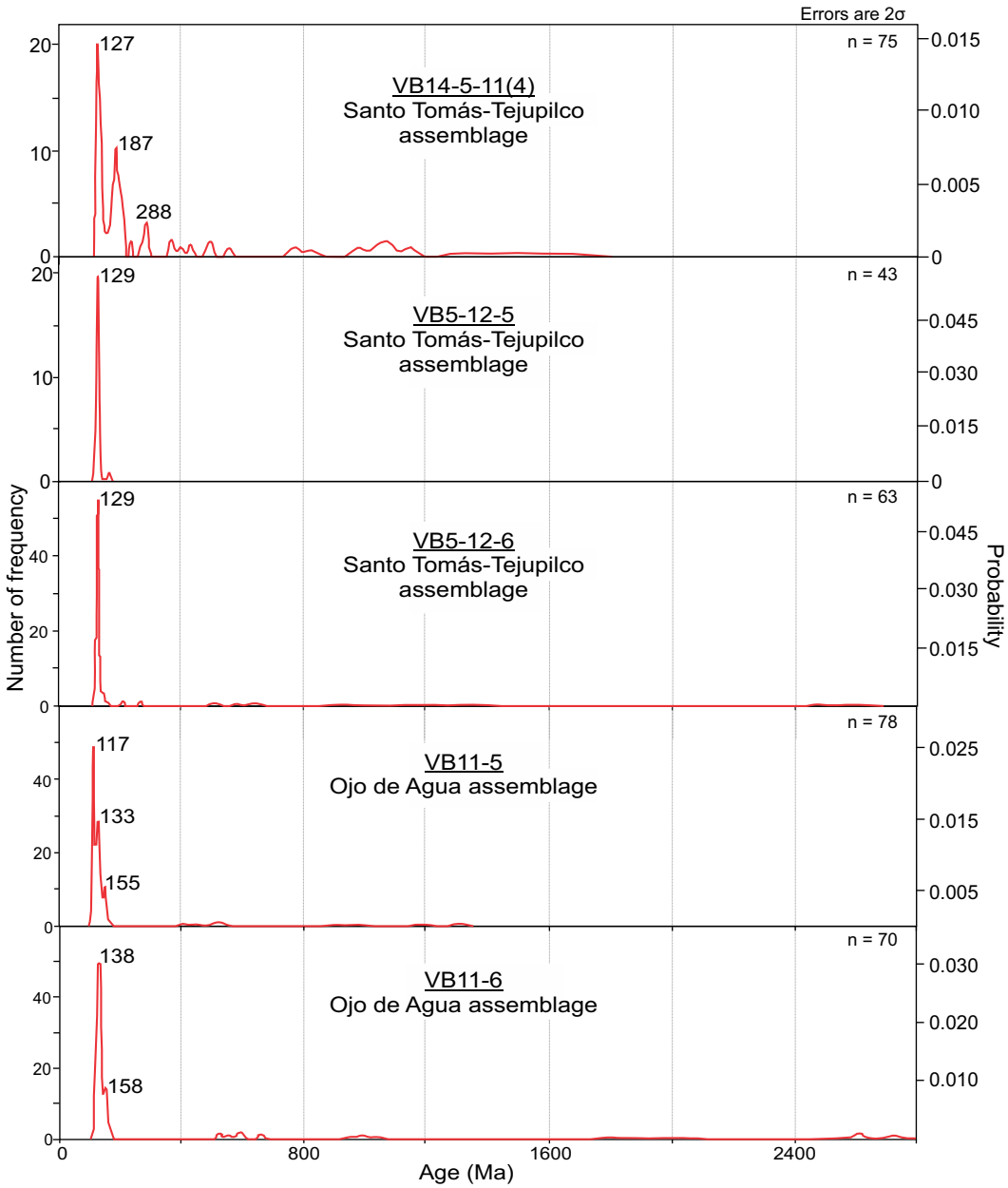

Figure 10. Probability density plots obtained for dated metasandstones from the Santo Tomás–Tejupilco and Ojo de Agua assemblages. Sample locations are given in Figure 4 and Table 3.

Aptian Teloloapan and the Albian–Cenomanian Palmar Chico assemblages, respectively. This scenario implies that the Santo Tomás–Tejupilco and Arcelia assemblages were deposited in a relatively narrow, intraoceanic basin within the Guerrero terrane, receiving detritus from the two arc massifs. This is in contrast with the paleogeographic reconstruction of the Arperos Basin at Guanajuato. In fact, in central Mexico, petrologic data indicate that the Arperos Basin was bounded by the North American continental mainland to the east and an Upper Jurassic–Lower Cretaceous arc assemblage of the Guerrero terrane to the west. Such a paleogeographic conflict can be resolved in light of our new geochronologic data. The 100.9 Ma $^{40}Ar/^{39}Ar$ isochron age obtained for a metabasalt from the Palmar Chico assemblage is in agreement with the previous Albian–Cenomanian age range inferred for this arc succession (Delgado-Argote et al., 1992; Elías-Herrera et al., 2000). However, the 129.5 Ma rhyolitic dike crosscutting the analyzed metabasaltic flow indicates that $^{40}Ar/^{39}Ar$ ages reflect Ar loss and resetting and call for a substantial reinterpretation of the previous isotopic ages. In light of these data, the Teloloapan and Palmar Chico assemblages overlap in age and contain similar submarine arc successions that overlie the Santo Tomás–Tejupilco and Arcelia assemblages with a top-to-the-NE main direction of tectonic transport (Freydier et al., 1996; Elías-Herrera, 2004; Fitz-Díaz et al., 2008; this work) (Fig. 12). Therefore, we interpret the Teloloapan and Palmar Chico assemblages as two isolated exposures of the same allochthonous volcanic massif, which was originally located southwest of the Santo Tomás–Tejupilco and Arcelia assemblages and was subsequently detached from its basement and tectonically transported to the NE during its collision with the North American mainland margin (Figs. 12 and 13B). Considering such a

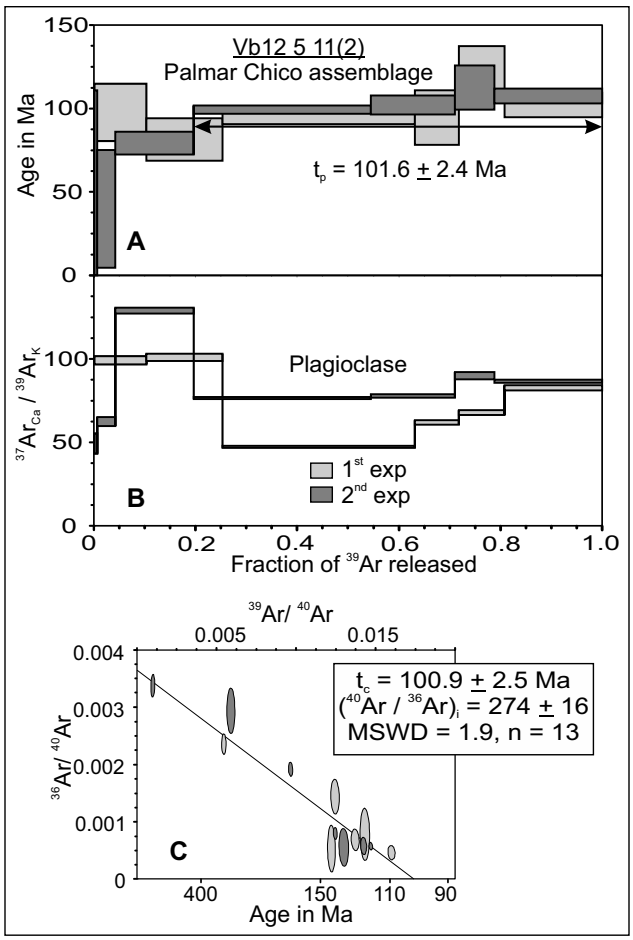

Figure 11. ^{40}Ar-^{39}Ar results obtained for a plagioclase concentrate from metabasalt VB12-5-11(2). (A) Age spectra and plateau age (t_p) calculated with the weighted mean of the four fractions identified by the arrow. The uncertainty of the plateau age given in the figure includes the goodness of fit of the weighted mean and the uncertainty in J. (B) $^{37}Ar_{Ca}/^{39}Ar_K$ diagram indicating that the plagioclase is calcium rich. (C) $^{36}Ar/^{40}Ar$ versus $^{39}Ar/^{40}Ar$ correlation diagram. The uncertainty of isochron age (t_c) given in the figure includes the goodness of fit of the best straight line and the uncertainty of J. MSWD—mean square of weighted deviates.

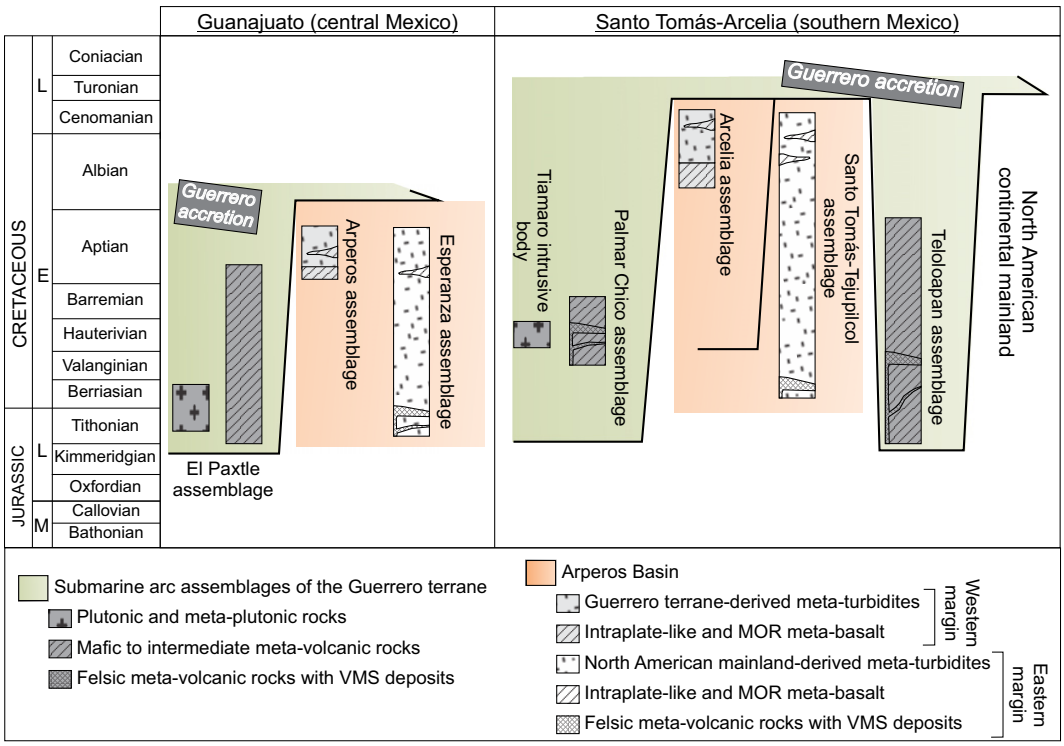

Figure 12. Chronostratigraphic columns of the Guanajuato and Santo Tomás–Arcelia areas. Both areas display a comparable tectono-stratigraphic architecture, which is characterized by Upper Jurassic–Lower Cretaceous primitive arc assemblages (El Paxtle, Palmar Chico, and Teloloapan arc assemblages) tectonically emplaced on the highly tectonized Tithonian–Cenomanian Arperos Basin. The Arperos Basin displays a marked provenance asymmetry: North American mainland-sourced sedimentary rocks were deposited at its eastern side (Esperanza and Santo Tomás–Tejupilco assemblages), whereas terrigenous rocks derived from the Guerrero terrane developed at its western side (Arperos and Arcelia assemblages). E—Early; M—Middle; L—Late.

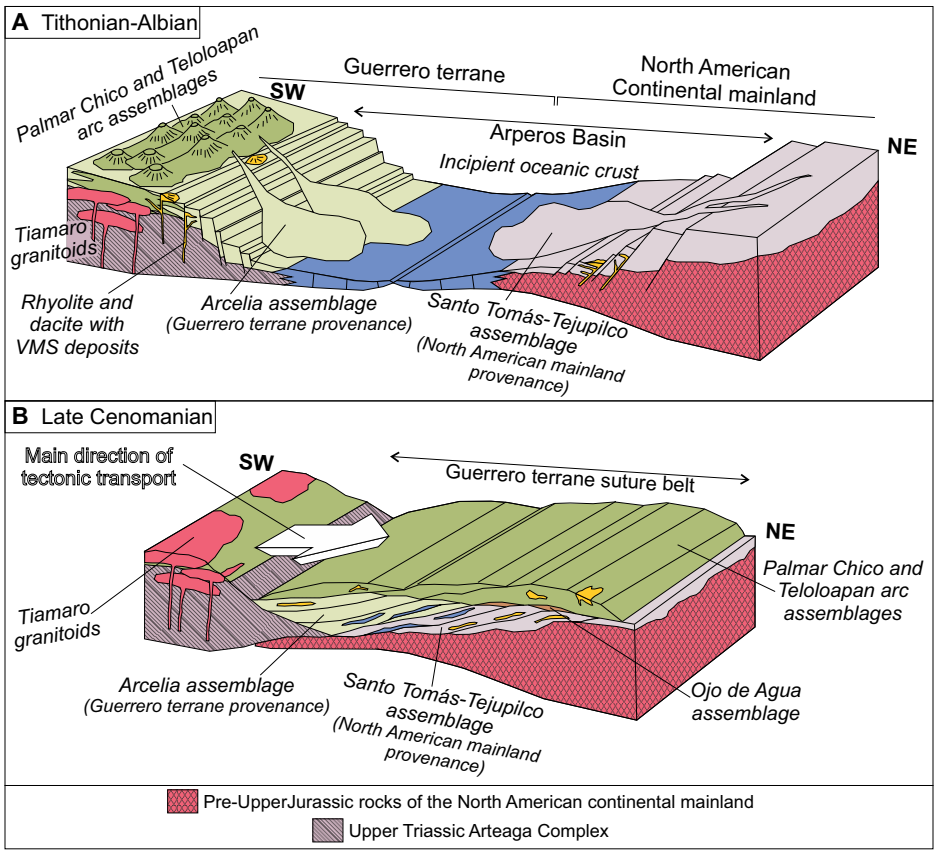

Figure 13. Two-step schematic evolution of the Arperos Basin in southern Mexico. (A) Between the Tithonian and the Albian, the North American mainland-sourced turbidites of the Santo Tomás–Tejupilco assemblage were deposited at the eastern side of the Arperos Basin. The western side of the Arperos Basin was dominated by accumulation of turbidites derived from the mafic to intermediate volcanic sources of the Guerrero terrane (Arcelia assemblage). Sedimentation in the Arperos Basin was coeval with the emplacement of Upper Jurassic–Early Lower Cretaceous rhyodacitic dikes and lava flows hosting volcanogenic massive sulfide (VMS) deposits and Aptian–lower Cenomanian intraplate-like and mid-ocean ridge (MOR) basalts, which are interpreted as the result of the progressive backarc continental extension and subsequent oceanic spreading. (B) During the Cenomanian, the Arperos Basin collapsed and was closed, producing the top-to-the-NE emplacement of the Palmar Chico–Teloloapan arc assemblage on the volcano-sedimentary basinal succession.

scenario, the ca. 130 Ma pluton exposed in the surroundings of Tiamaro can be interpreted as an exposure of the arc roots, which were exhumed during detachment and accretion of the volcanic massif (Fig. 13B).

In synthesis, petrologic and geochronologic data presented in this work document that the paleogeographic reconstruction proposed for the Guanajuato area can be extended in southern Mexico as originally proposed by Freydier et al. (1996), and these data indicate that the Arperos Basin represented a main morphological feature during the Late Jurassic–Early Cretaceous that separated the arc assemblages of the Guerrero terrane from the North American continental mainland.

NORTH AMERICAN VERSUS PACIFIC ORIGIN OF THE ARPEROS BASIN AND GUERRERO TERRANE

Our stratigraphic and petrologic data suggest that the volcano-sedimentary successions exposed at Guanajuato and in the Santo Tomás–Arcelia area can be ascribed to the Arperos Basin. Volcanic and volcaniclastic rocks within the Arperos Basin document that sedimentation was coeval with intrabasinal magmatic activity. In fact, rhyodacitic dikes and volcanic flows hosting VMS deposits were emplaced along the Guerrero terrane and continental mainland margins during the Tithonian and lower Early Cretaceous (Mortensen et al., 2008; Elías-Herrera et al., 2009; Martini et al., 2011; this work), whereas intraplate-like and MOR basaltic flows dominated in the Aptian–Cenomanian (Freydier et al., 1996; Elías-Herrera et al., 2000; Talavera-Mendoza et al., 2007; Martini et al., 2011) (Figs. 12 and 13A). Felsic dikes and lava flows are peraluminous and ubiquitously contain Paleozoic and Precambrian inherited zircons (Mortensen et al., 2008; Martini et al., 2011; this work), which suggests that, at least during the Tithonian and lower Early Cretaceous, the Arperos Basin was still floored by continental or continental-recycled rocks. Spreading within the Arperos Basin and development of an oceanic substrate are constrained in the Aptian–Cenomanian by the age of the intraplate-like and MOR basaltic flows (Freydier et al., 1996; Elías-Herrera et al., 2000; Talavera-Mendoza et al., 2007; Martini et al., 2011). According to this scenario, the Tithonian inception of the Palmar Chico–Teloloapan arc took place when the eastern boundary of the Guerrero terrane was still in close proximity to the North American continental mainland, and oceanic crust was not yet formed in the Arperos Basin. Based on this consideration, the Pacific hypothesis on the origin of the Guerrero terrane can be discarded, because it implies that the Palmar Chico and Teloloapan arc assemblages developed separately from the North American continental mainland as a result of the subduction of the Arperos Basin oceanic substrate (e.g., Tardy et al., 1994; Dickinson and Lawton, 2001; Talavera-Mendoza et al., 2007) (Figs. 2A and 2B). In agreement with the paleogeographic reconstruction proposed for the Guanajuato area, our data favor the idea that the Palmar Chico and Teloloapan assemblages represent the vestiges of a west-facing North American arc, which formed on top of the Upper Triassic Arteaga Complex and was bounded to the east by the backarc Arperos Basin (Fig. 2C). The westward rifting of the Palmar Chico–Teloloapan arc and separation from the North American mainland were triggered by the oceanic spreading in the backarc basin, which subsequently collapsed and led to backarc inversion and accretion of the Guerrero terrane arc back to nuclear Mexico.

CONCLUSIONS

Data presented in this paper permit the reconstruction of the backarc Arperos Basin in southern Mexico. In analogy with present-day continent-influenced backarc basins, metasandstone provenance analysis documents that sedimentation within the Arperos Basin occurred asymmetrically: North American continent-recycled sediments were deposited

on the eastern side, whereas Guerrero terrane arc-derived clastic sediments dominated on the western side. Sedimentation in the Arperos Basin was coeval with the emplacement of Upper Jurassic–lowermost Cretaceous rhyodacitic dikes and lava flows hosting VMS deposits, and Aptian–lower Cenomanian intraplate-like and MOR basalts. These volcanic rocks are interpreted as the result of the progressive backarc continental extension and subsequent oceanic spreading. Based on these data, the Arperos Basin evolved progressively from continentally to oceanic floored during the Early Cretaceous, suggesting that a mature backarc oceanic crust was generated only ca. 15 Ma before the Guerrero terrane accretion. These data suggest that the Guerrero terrane represents a detached slice of the North American continental margin that was rifted during backarc spreading and subsequently accreted back to nuclear Mexico.

ACKNOWLEDGMENTS

This research was funded by PAPIIT (Programa de Apoyo a Proyectos de Investigación e Innovación Tecnológica) grants IN110810-3 to Antoni Camprubí and CONACyT (Consejo Nacional de Ciencia y Tecnología) CB164454 to Fernando Ortega-Gutiérrez. Joaquín Aparicio (Instituto de Geología, Universidad Nacional Autónoma de México [UNAM]) prepared thin sections. Carlos Ortega-Obregón (Laboratorio de Estudios Isotópicos, Centro de Geociencias, UNAM) performed zircon isotopic analyses. The helpful comments and suggestions of two anonymous reviewers improved the manuscript.

REFERENCES CITED

Abascal, G., and Murillo-Muñetón, G., 2013, Preliminary sequence stratigraphy: Framework of the SW part of the Actopan Platform, Lower Cretaceous, Hidalgo, Mexico: Cancun, Mexico, American Geophysical Union, Meeting of the Americas, Abstracts with Programs.

Barboza-Gudiño, J.R., Orozco-Esquivel, M.T., Gómez-Anguiano, M., and Zavala-Monsiváis, A., 2008, The Early Mesozoic volcanic arc of western North America in northeastern Mexico: Journal of South American Earth Sciences, v. 25, p. 49–63, doi:10.1016/j.jsames.2007.08.003.

Barboza-Gudiño, J.R., Zavala-Monsiváis, A., Venegas-Rodríguez, G., and Barajas-Nigoche, L.D., 2010, Late Triassic stratigraphy and facies from northeastern Mexico: Tectonic setting and provenance: Geosphere, v. 6, p. 621–640, doi:10.1130/GES00545.1.

Bartolini, C., and Spell, T., 1997, An early Jurassic age ($^{40}Ar/^{39}Ar$) for the Nazas Formation at the Cañada Villa Juárez, northeastern Durango, México: El Paso, Texas, Geological Society of America Abstracts with Programs.

Cabral-Cano, E., Lang, H.R., and Harrison, C.G.A., 2000, Stratigraphic assessment of the Arcelia-Teloloapan area, southern Mexico: Implication for southern Mexico's post-Neocomian tectonic evolution: Journal of South American Earth Sciences, v. 13, p. 443–457, doi:10.1016/S0895-9811(00)00035-3.

Campa, M.F., and Coney, P.J., 1983, Tectono-stratigraphic terranes and mineral resource distribution in Mexico: Canadian Journal of Earth Sciences, v. 20, p. 1040–1051, doi:10.1139/e83-094.

Campa-Uranga, M.F., Torres-de León, R., Iriondo, A., and Premo, W.R., 2012, Caracterización geológica de los ensambles metamórficos de Taxco y Taxco el Viejo, Guerrero, México: Boletín de la Sociedad Geológica Mexicana, v. 64, p. 369–385.

Cantú-Chapa, 1968, Las rocas eocretácicas de Zitácuaro, Michoacán, Monografía del Instituto Mexicano del Petróleo, Tecnología de la Exploración: Sección Geología, v. 2, p. 3–18.

Centeno-García, E., 2005, Review of upper Paleozoic and lower Mesozoic stratigraphy and depositional environments of central and west Mexico: Constraints on terrane analysis and paleogeography, *in* Anderson, T.H., Nourse, J.A., McKee, J.W., and Steiner, M.B., eds., The Mojave-Sonora Megashear Hypothesis: Development, Assessment, and Alternatives: Geological Society of America Special Paper 393, p. 233–258.

Centeno-García, E., Corona-Chávez, P., Talavera-Mendoza, O., and Iriondo, A., 2003, Geologic and tectonic evolution of the western Guerrero terrane—A transect from Puerto Vallarta to Zihuatanejo, Mexico, *in* Alcayde, M., and Gómez-Caballero, A., eds., Geologic Transects across Cordilleran Mexico: Puerto Vallarta, Jalisco, Mexico, Guidebook for the Field Trips of the 99th Geological Society of America Cordilleran Section Annual Meeting, April 4–7, 2003, Universidad Nacional Autónoma de México, Instituto de Geología, Special Paper 1, p. 201–228.

Centeno-García, E., Guerrero-Suástegui, M., and Talvera-Mendonza, O., 2008, The Guerrero Composite terrane of western Mexico: Collision and subsequent rifting in a suprasubduction zone, *in* Draut, A., Clift, P.D., and Scholl, D.W., eds., Formation and Application of the Sedimentary Record in Arc Collision Zones: Geological Society of America Special Paper 436, p. 279–308.

Chiodi, M., Monod, O., Busnardo, R., Gaspard, D., Sánchez, A., and Yta, M., 1988, Une descordance anté-albienne datée par una faune d'ammonites et de brachiopods de type thétisien au Mexique central: Geobios, v. 21, p. 125–135, doi:10.1016/S0016-6995(88)80014-7.

Coney, P.J., Jones, D.L., and Monger, J.W.H., 1980, Cordilleran suspect terranes: Nature, v. 288, p. 329–333, doi:10.1038/288329a0.

Connelly, J.N., 2001, Degree of preservation of igneous zonation in zircon as a signpost for concordancy in U/Pb geochronology: Chemical Geology, v. 172, p. 25–39, doi:10.1016/S0009-2541(00)00234-5.

Corfu, F., Hanchar, J.M., Hoskin, P.W.O., and Kinny, P., 2003, Atlas of zircon textures: Reviews in Mineralogy and Geochemistry, v. 53, p. 469–500, doi:10.2113/0530469.

Critelli, S., La Pera, E., and Ingersoll, R.V., 1997, The effects of source lithology, transport, deposition and sampling on the composition of southern California sand: Sedimentology, v. 44, p. 653–671, doi:10.1046/j.1365-3091.1997.d01-42.x.

Dávila-Alcocer, V.M., and Guerrero-Suástegui, M., 1990, Una edad basada en radiolarios para la secuencia volcanosedimentaria al oriente de Arcelia, estado de Guerrero: México D.F., 10ª Convención de la Sociedad Geológica Mexicana, Memoria de Resúmenes, p. 83.

Delgado-Argote, L.A., López-Martínez, M., York, D., and Hall, C.M., 1992, Geologic framework and geochronology of ultramafic complexes of southern Mexico: Canadian Journal of Earth Sciences, v. 29, p. 1590–1604, doi:10.1139/e92-125.

Dickinson, W., and Lawton, T., 2001, Carbonaceous to Cretaceous assembly and fragmentation of Mexico: Geological Society of America Bulletin, v. 113, p. 1142–1160, doi:10.1130/0016-7606(2001)113<1142:CTCAAF>2.0.CO;2.

Dickinson, W.R., 1970, Interpreting detrital modes of greywacke and arkose: Journal of Sedimentary Petrology, v. 40, p. 695–707.

Dickinson, W.R., 1985, Interpreting provenance relations from detrital modes of sandstones, *in* Zuffa, G.G., Provenance of Arenites: Dordrecht, Netherlands, North Atlantic Treaty Orgaization, Advanced Study Institute Series 148, p. 332–361.

Dickinson, W.R., and Suczek, C.A., 1979, Plate tectonics and sandstone composition: The American Association of Petroleum Geologists Bulletin, v. 63, p. 2164–2172.

Elías-Herrera, M., 2004, Geología Precenozoica de la región de Tejupilco, Estado de México, y sus implicaciones tectónicas [Ph.D. thesis]: México D.F., Instituto de Geología, Universidad Nacional Autónoma de México.

Elías-Herrera, M., Sánchez-Zavala, J.L., and Macias-Romo, C., 2000, Geologic and geochronologic data from the Guerrero terrane in the Tejupilco area, southern Mexico: New constraints on its tectonic interpretation: Journal of South American Earth Sciences, v. 13, p. 355–375, doi:10.1016/S0895-9811(00)00029-8.

Elías-Herrera, M., Ortega-Gutiérrez, F., Macías-Romo, C., Sánchez-Zavala, J.L., and Solari, L.A., 2009, Geocronología U-Pb del Esquisto Tejupilco: Implicaciones tectónicas prealbianas para el terreno Guerrero, sur de México: Simposio: Taxco, Guerrero, México, "El origen, naturaleza y evolución geológica del Terreno Guerrero y sus conexiones regionals."

Fitz-Díaz, E., Tolson, G., Camprubí, A., Rubio-Ramos, M.A., and Prol-Ledesma, R.M., 2008, Deformación, vetas, inclusiones fluidas y la evolución tectónica de las rocas cretácicas de Valle de Bravo, Estado de México, México: Revista Mexicana de Ciencias Geológicas, v. 25, no. 1, p. 59–81.

Folk, R.L., 1974, Petrology of Sedimentary Rocks: Austin, Texas, Hemphill Publishing Company, 182 p.

Freydier, C., Martinez, R., Lapierre, H., Tardy, M., and Coulon, C., 1996, The Early Cretaceous Arperos oceanic basin (western Mexico): Geochemical evidence for an aseismic ridge formed near a spreading center: Tectonophysics, v. 259, p. 343–367, doi:10.1016/0040-1951(95)00143-3.

Garza-González, C.E., 2007, Metalogenia del porfido de cobre de Tiámaro, Estado de Michoacán [Ph.D. thesis]: Juriquilla, Centro de Geociencias, Universidad Nacional Autónoma de México.

Gazzi, P., 1966, Le arenarie del flysch sopracretaceo dell' Appennino modenese: Correlazioni con il flysch di Monghidoro: Mineralogica e Petrografica Acta, v. 12, p. 69–97.

Gehrels, G., 2011, Detrital zircon U-Pb geochronology: Current methods and new opportunities, *in* Busby, C., and Azor-Pérez, A., eds., Recent Advances in Tectonics of Sedimentary Basins: Chichester, UK, John Wiley and Sons, 664 p., doi:10.1002/9781444347166.ch2.

Gehrels, G., Valencia, V., and Pullen, A., 2006, Detrital zircon geochronology by laser ablation multicollector ICPMS at the Arizona LaserChron Center, *in* Olszewski, T., ed., Geochronology: Emerging Opportunities: The Paleontological Society Papers 12, p. 67–76.

Harris, A., Allen, C., Bryan, S., Campbell, I., Holcombe, R., and Palin, J., 2004, ELA-ICP-MS U-Pb zircon geochronology of regional volcanism hosting the Bajo de la Alumbrera Cu-Au deposit: Implications for porphyry-related mineralization: Mineralium Deposita, v. 39, p. 46–67, doi:10.1007/s00126-003-0381-0.

Ingersoll, R.V., and Suczek, C.A., 1979, Petrology and provenance of Neogene sand from Nicobar and Bengal Fans, DSDP sites 211 and 218: Journal of Sedimentary Petrology, v. 49, p. 1217–1228.

Ingersoll, R.V., Bullard, T.F., Ford, R.L., Grimm, J.P., Pickle, J.D., and Sares, S.W., 1984, The effect of grain size on detrital modes: A test of the Gazzi-Dickinson point-counting method: Journal of Sedimentary Petrology, v. 54, no. 1, p. 103–116.

Israde-Alcantara, I., and Martinez-Alvarado, M.L., 1986, Contribución al Estudio Geológico de la Transición Pacífico-Tethis en el Área de Zitácuaro, Michaocán [B.S. thesis]: Mexico D.F., Escuela Superior de Ingeniería y Arquitectura (ESIA), Instituto Politecnico Nacional.

Lapierre, H., Ortiz, L.E., Abouchami, W., Monod, O., Coulon, C., and Zimmermann, J.L., 1992, A crustal section of an intra-oceanic island arc: The Late Jurassic–Early Cretaceous Guanajuato magmatic sequence, central Mexico: Earth and Planetary Science Letters, v. 108, p. 61–77, doi:10.1016/0012-821X(92)90060-9.

Ludwig, K.R., 2004, Isoplot/Ex, version. 3, A geochronological toolkit for Microsoft Excel: Berkeley Geochronology Center, Publication no. 4.

Martínez-Reyes, J., 1992, Mapa geológico de la Sierra de Guanajuato con resumen de la geología de la Sierra de Guanajuato: Mexico D.F., Universidad Nacional Autónoma de México, Instituto de Geología, Cartas Geológicas y Mineras 8.

Martini, M., Ferrari, L., López-Martínez, M., Cerca-Martínez, M., Valencia, V., and Serrano-Duran, L., 2009, Cretaceous–Eocene magmatism and Laramide deformation in southwestern Mexico: No role for terrane accretion, *in* Kay, S.M., Ramos, V.A., and Dickinson, W.R., Backbone of the Americas: Shallow Subduction, Plateau Uplift, and Ridge and Terrane Collision: Geological Society of America Memoir 204, p. 151–182.

Martini, M., Mori, L., Solari, L., and Centeno-García, E., 2011, Sandstone provenance of the Arperos Basin (Sierra de Guanajuato, central Mexico): Late Jurassic–Early Cretaceous back-arc spreading as the foundation of the Guerrero terrane: The Journal of Geology, v. 119, p. 597–617, doi:10.1086/661989.

Martini, M., Fitz, E., Solari, L., Camprubí, A., Hudleston, P.J., Lawton, T.F., Tolson, G., and Centeno-García, E., 2012, The Late Cretaceous evolution of the Mexican Fold-Thrust Belt and its possible relationship to the accretion of the Guerrero Terrane, *in* Aranda-Gómez, J.J., Tolson, G., Molina-Garza, R.S., The Southern Cordillera and Beyond: Geological Society of America Field Trip Guide 25, p. 20–38.

Martini, M., Solari, L., and Camprubí, A., 2013, Kinematics of the Guerrero terrane accretion in the Sierra de Guanajuato, central Mexico: New insights for the structural evolution of arc-continent collisional zones: International Geology Review, v. 55, no. 5, p. 574–589, doi:10.1080/00206814.2012.729361.

Mendoza, O.T., and Suástegui, M.G., 2000, Geochemistry and isotopic composition of the Guerrero Terrane (western Mexico): Implication for the tectono-magmatic evolution of southwestern North America during the Late Mesozoic: Journal of South American Earth Sciences, v. 13, p. 297–324, doi:10.1016/S0895-9811(00)00026-2.

Mortensen, J.K., Hall, B.V., Bissig, T., Friedman, R.M., Danielson, T., Oliver, J., Rhys, D.A., Ross, K.V., and Gabites, J.E., 2008, Age and paleotectonic setting of volcanogenic massive sulphide deposits in the Guerrero terrane of Central Mexico: Constraints from U-Pb age and Pb isotope studies: Economic Geology and the Bulletin of the Society of Economic Geologists, v. 103, p. 117–140.

Ortega-Flores, B., Solari, L., Lawton, T.F., and Ortega-Obregón, C., 2014, Detrital-zircon record of major Middle Triassic–Early Cretaceous provenance shift, central Mexico: Demise of Gondwanan continental fluvial systems and onset of back-arc volcanism and sedimentation: International Geology Review, v. 56, no. 2, p. 237–261, doi:10.1080/00206814.2013.844313.

Ortíz-Hernandez, E.L., Chiodi, M., Lapierre, H., Monod, O., and Calvet, P., 1992, El arco intraoceánico alóctono (Cretácico Inferior) de Guanajuato-características petrográficas, geoquímicas, estructurales e isotópicas del complejo filonianao y de las lavas basálticas asociadas, implicaciones geodinámicas, Revista del Instituto de Geología: Universidad Nacional Autónoma de México, v. 9, no. 2, p. 126–145.

Palacios-García, N.B., and Martini, M., 2014, From back-arc rifting to arc accretion: The Late Jurassic–Early Cretaceous evolution of the Guerrero terrane recorded by a major provenance change in sandstones from the Sierra de los Cuarzos area, central Mexico: International Geology Review, v. 56, no. 11, p. 1377–1394, doi:10.1080/00206814.2014.938367.

Rubatto, D., 2002, Zircon trace element geochemistry: partitioning with garnet and the link between U-Pb ages and metamorphism: Chemical Geology, v. 184, p. 123–138, doi:10.1016/S0009-2541(01)00355-2.

Rubio-Cisneros, I.I., and Lawton, T.F., 2011, Detrital zircon U-Pb ages of sandstones in continental red beds at Valle de Huizachal, Tamaulipas, NE Mexico: Record of Early-Middle Jurassic arc volcanism and transition to crustal extension: Geosphere, v. 7, p. 159–170, doi:10.1130/GES00567.1.

Salinas-Prieto, J.C., Monod, O., and Faure, M., 2000, Ductile deformations of opposite vergence in the eastern part of the Guerrero terrane (SW Mexico): Journal of South American Earth Sciences, v. 13, p. 389–402, doi:10.1016/S0895-9811(00)00031-6.

Talavera-Mendoza, O., Ruiz, J., Gehrels, G.E., Valencia, V.A., and Centeno-García, E., 2007, Detrital zircon U/Pb geochronology of southern Guerrero and western Mixteca arc successions (southern Mexico): New insights for the tectonic evolution of the southwestern North America during the late Mesozoic: Geological Society of America Bulletin, v. 119, p. 1052–1065, doi:10.1130/B26016.1.

Tardy, M., Lapierre, H., Freydier, C., Coulon, C., Gill, J.B., Mercier De Lepinay, B., Beck, C., Martinez, J., Talavera-Mendoza, O., Ortiz, E., Stein, G., Bourdier, J.L., and Yta, M., 1994, The Guerrero suspect terrane (western Mexico) and coeval arc terranes (the Greater Antilles and the Western Cordillera of Colombia): A late Mesozoic intra-oceanic arc accreted to cratonal America during the Cretaceous: Tectonophysics, v. 230, p. 49–73, doi:10.1016/0040-1951(94)90146-5.

Tera, F., and Wasserburg, G.J., 1972, U–Th–Pb systematics in three Apollo 14 basalts and the problem of initial Pb in lunar rocks: Earth and Planetary Science Letters, v. 14, p. 281–304, doi:10.1016/0012-821X(72)90128-8.

Zuffa, G.G., 1985, Optical analyses of arenites: Influence of methodology on compositional results, *in* Zuffa, G.G., Provenance of Arenites: Dordrecht, Netherlands, North Atlantic Treaty Organization, Advanced Study Institute Series 148, p. 165–189.